Molecular approach to alkali metal encapsulation by a PrussianBlueAnalogue Fe^{II}/Co^{III} cube in aqueous solution, kinetico-mechanistic exchange study.

Miguel A. Gonzálvez,[a,b] *Paul V. Bernhardt,*[a] *Mercè Font-Bardia,*[c] *Albert Gallen,*[b] *Jesús Jover,*[b,d] *Montserrat Ferrer,*[b,e*] *and Manuel Martínez* [b,e*]

[a] School of Chemistry and Molecular Biosciences, University of Queensland, Brisbane, Queensland 4072, Australia

[b] Secció de Química Inorgànica, Departament de Química Inorgànica i Orgànica. Universitat de Barcelona, Martí i Franquès 1-11, 08028 Barcelona, Spain

[c] Unitat de Difracció de Raigs-X. Centre Científic i Tecnològic de la Universitat de Barcelona. Universitat de Barcelona and Departament de Cristal·lografia, Mineralogia i Dipòsits Minerals. Facultat de Geologia, 08028 Barcelona, Spain

[d] Institut de Química Teòrica i Computacional (IQTC-UB), Universitat de Barcelona, 08028 Barcelona, Spain

[e] Institute of Nanoscience and Nanotechnology (IN2UB), Universitat de Barcelona, 08028 Barcelona, Spain

montse.ferrer@qi.ub.edu, manel.martinez@qi.ub.edu

Abstract

The preparation of a series of alkali metal inclusion complexes of the molecular cube $[\{Co^{III}(Me_3\text{-}tacn)\}_4\{Fe^{II}(CN)_6\}_4]\}]^{4-}$ (Me_3-tacn = 1,4,7-Trimethyl-1,4,7-triazacyclononane), a mixed valent Prussian Blue analogue bearing bridging cyanido ligands, has been achieved by following a redox-triggered self-assembly process. The molecular cubes are extremely robust and soluble in aqueous media ranging from 5 M $[H^+]$ to 2 M $[OH^-]$. All the complexes have been characterised by the standard MS, UV-Vis, ICP, multinuclear NMR spectroscopy and electrochemistry. Furthermore, XRD analyses of the sodium and lithium salts has also been achieved, and the inclusion of moieties of the form $\{M–OH_2\}^+$ (M = Li, Na) is confirmed. These inclusion complexes in aqueous solution are rather inert to cation exchange, and are characterised by a significant decrease in acidity due to hydrogen bonding inside the cubic cage. Exchange of the encapsulated cationic $\{M–OH_2\}^+$ or M^+ units by other alkali metals has also been studied from a kinetico-mechanistic perspective at different concentrations, temperatures, ionic strength and pressure. In all cases the thermal and pressure activation parameters obtained agree with a process that is dominated by differences in hydration of the cations entering and exiting the cage, although the size of the portal enabling the exchange also plays a determinant role, thus not allowing the large Cs^+ cation to enter. All the exchange substitutions studied follow a thermodynamic sequence that relates with the size and polarizing capability of the different alkali cations, although the process can be reversed allowing the entry of $\{Li–OH_2\}^+$ units on adsorption of the cube on an anion exchange resin and subsequent washing with Li^+ solution.

Introduction

Intensely coloured transition metal mixed valence complexes such as Prussian Blue (or ferric ferrocyanide) have attracted the attention of both the chemical and general public communities for centuries. In fact, the general use of Prussian Blue as a resistant and fairly innocuous inorganic colorant cannot be overstated. As mixed valence compounds, **P**russian **B**lue **A**nalogues (PBAs) have been used academically for the establishment of fundamental mixed valent classifications related to electronic coupling between the metal centres and the symmetry-allowed inner-sphere optical electron transfer occurring between them.[1-8] In reactivity aspects, these species have been utilised as cheap, metal abundant-catalysts in water oxidation processes[9-10] and in electrochemical applications.[11] Recently, the use of this type of complexes in the development of photomagnetic switching materials has also been developed by several groups.[12-16] Furthermore, both anionic Prussian Blue and PBAs are also know to acts as hosts for cationic guests in general, which has led to various applications.[14, 17-24] Their use as sequestering agents has been explored, although their ion exchange properties in aqueous solution are difficult to measure. Crown ether ligands offer a good perspective in this respect,[25] but the lability of their complexes in aqueous solution hampers their 'controlled' sequestering/bleaching reactions.[26] The use and applicability of PBAs in medicinal chemistry has also been recently reviewed.[27]

The boundaries between discrete molecular, polymeric and solid state PBAs are rather diffuse.[12, 28-30] In this respect, solubility plays also a crucial role in the development and use of this type of compounds, especially when water is the solvent of choice, as recommended in Green Chemistry applications. In general, these compounds tend to become less soluble as their nuclearity increases. Furthermore, the solubility/stability issues of discrete molecular PBAs tend to require aprotic and non-coordinating solvents, to avoid destruction of the 2D or 3D structures due to the substitution lability of the metal centres.[30-31] The possible use of PBAs as electron reservoirs/sinks is also an important point to be considered for their applications.[10, 23, 32] For these purposes, the compounds require substitution inertness to avoid dissociation and loss of the components of this functional assembly.

Synthesis of PBAs in a controlled and reproducible manner is vital for any future application. Many members of this family are isolated as crystalline but insoluble polymeric compounds (metal-organic frameworks) with well-defined structures based on XRD data, but the establishment of the precise and rational preparative conditions is challenging. Alternative preparative procedures involving designed self-assembly aim to avoid such difficulties. The validity of the approach has been proved in a wealth of occasions for several families of compounds.[33-34] We have been involved for some time in the study of the self-assembly and reactivity of 3D oligonuclear structures, including the study of their formation and dynamic behaviour.[35-38] A concerted redox-triggered ligand substitution approach has led to the family of the complexes indicated in Chart 1 where cyanido ligands bridge the metal centres and the remaining coordination sites are occupied by a macrocyclic tri-, tetra- or pentaamine (N_3, N_4 or N_5).[39-45] These Co/Fe PBAs behave as discrete molecular Class II mixed-valence complexes with remarkable thermal and pH stability, as well as reversible redox reactivity,[44, 46-49] and this chemistry has successfully included other

metals as well.[40, 50-52] The potential applications of the redox properties of these complexes on inert supports have also been explored.[53-54]

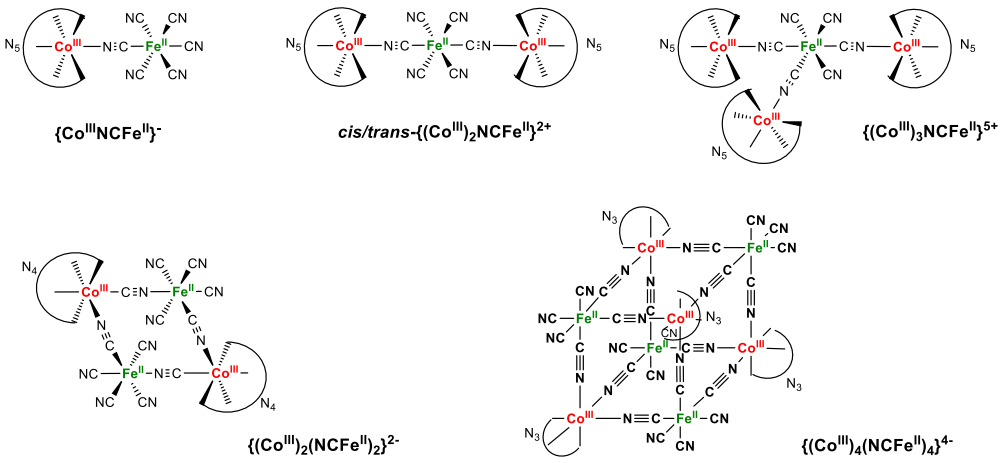

Chart 1

In this report we focus on the inclusion properties of the recently communicated molecular cube in Chart 1 (N_3 = 1,4,7-trimethyl-1,4,7-triazacyclononane, Me_3-tacn).[45] The alkali metal and water exchange properties have been studied by time resolved UV-Vis spectroscopy and multinuclear NMR measurements at variable concentrations, ionic strength, temperature and pressure in order to obtain the activation parameters for the process. These proved to be dominated by solvation/de-solvation of the different cations on exiting/entering (aquation/anation) the cubic cage. This is a fact that had not been explored so far precisely because the lack of the desirable aqueous chemistry of these molecular PBAs. Furthermore, we observed a particularly unexpected reactivity on chromatography-adsorbed samples, which was not paralleled in solution. This reveals an interesting heterogeneous effect on the encapsulation reactivity of the highly negatively charged cubic structure. DFT calculations have been employed to assess the structural features of the cubic complexes with encapsulated alkaline cations containing different numbers of water molecules.

Results

Preparation of compounds

The lithium, sodium and potassium salts of the $[\{Co^{III}(Me_3\text{-tacn})\}_4\{Fe^{II}(CN)_6\}_4]^{4-}$ mixed valence molecular cubes have been prepared using the well-developed mechanistically directed self-assembly process described in previous literature reports for 2D structures (Chart 1).[39, 41-44, 49, 51, 55] A preliminary communication on the preparation of the sodium and potassium salts of the cube has also been reported.[45] In all cases the preparations have been conducted, as indicated in the experimental section, by reaction of $[Co^{III}(Me_3\text{-tacn})Cl_3]$, with the desired $[Fe^{II}(CN)_6]^{4-}$ salt in aqueous solution at 50 ºC overnight. From this point, the solutions were treated as indicated below to obtain the various salts of the mixed-valence cube.

Lithium salt

The procedure for the obtention of the lithium salt of $[\{Co^{III}(Me_3\text{-tacn})\}_4\{Fe^{II}(CN)_6\}_4]^{4-}$ parallels that used for the reported preparation of its sodium or potassium salts,[45] but using (see experimental part) $Li_4[Fe^{II}(CN)_6]$ as the source of the $\{Fe^{II}(CN)_6\}$ building block. An initial Sephadex G-25 chromatographic workup, to eliminate any excess of cobalt or iron building blocks, produced a purple solution that, after being taken to dryness at 35-45 ºC, exhibits a ^{1}H NMR spectrum with signals of the symmetric $\{Co^{III}(Me_3\text{-tacn})\}$ moiety *plus* significant peaks of low intensity (with respect to those of the Me_3-tacn moiety) at 4.21 and 3.87 ppm (Figure 1a).[56] The signal at 3.87 ppm is associated with water bound to residual amounts of Na^+ in the building block samples, which led to the formation of the already described sodium salt of the cubic structure.[45] As for the signal at 4.21 ppm, it shows a very distinct lineshape that is associated to the coupling to a $I = 3/2$ spin nucleus in a very symmetrical environment, as expected for a small ^{7}Li centre ($J_{H\text{-}Li}$ = 1.1 Hz). Furthermore, the chemical shift (4.21 ppm), compared with that of encapsulated $\{Na–OH_2\}^+$ (3.87 ppm), is consistent with a more acidic water molecule, as expected from the higher polarising power of the attached lithium cation. In this respect, the ^{7}Li NMR spectrum of the same sample shows a signal at 0 ppm, from aquated lithium cations, *plus* a triplet at 0.09 ppm ($J_{Li\text{-}H}$ = 1.1 Hz) (Figure 1b) indicative of the presence of an encapsulated $\{Li–OH_2\}^+$ unit. Figure 2a shows the DOSY NMR spectrum of the same sample, which corroborates the inclusion of either the $\{Li–OH_2\}^+$ (4.21 ppm) or $\{Na–OH_2\}^+$ (3.87 ppm) units within their corresponding cages. The ^{13}C NMR spectrum of the same sample is even more revealing, showing the presence of three sets of resonances in the cyanide region corresponding to cubic structures, *plus* that of the remaining $[Fe^{II}(CN)_6]^{4-}$, still present in the crude mixture obtained under the experimental conditions used (Figure 2b).

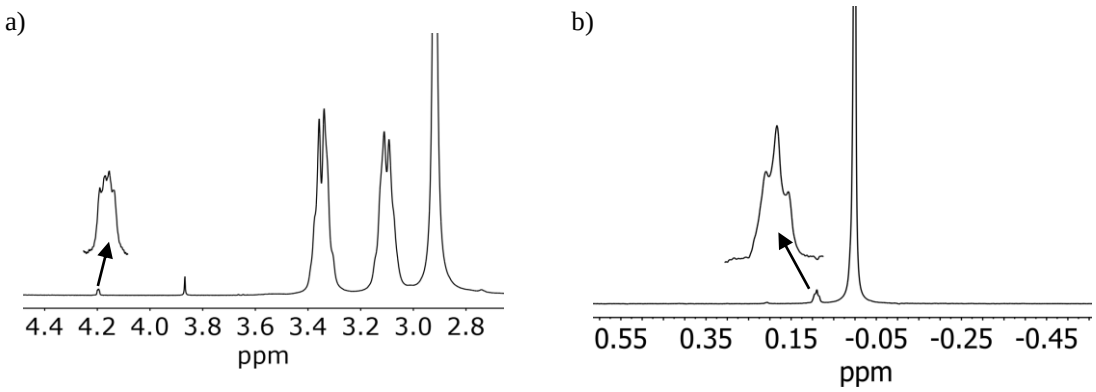

Figure 1.- a) ^{1}H NMR spectrum of the Sephadex G-25 eluate obtained from the crude mixture of the preparation of the lithium salt of the $[\{Co^{III}(Me_3\text{-tacn})\}_4\{Fe^{II}(CN)_6\}_4]^{4-}$ cubic cage; b) ^{7}Li NMR spectrum of the same sample.

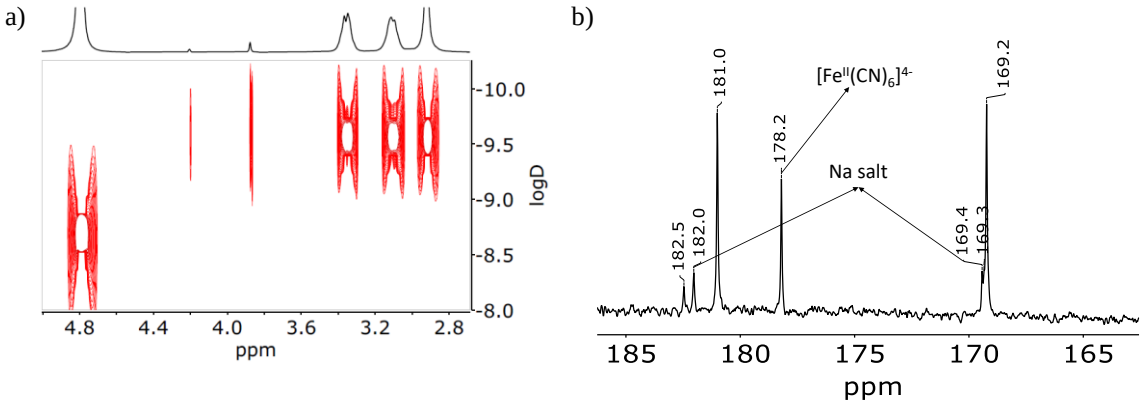

Figure 2.- a) DOSY spectrum of the sample obtained from the crude mixture of the preparation of the lithium salt of the $[\{Co^{III}(Me_3\text{-tacn})\}_4\{Fe^{II}(CN)_6\}_4]^{4-}$ structure. b) ^{13}C NMR spectrum of the same sample.

The ^{1}H and ^{7}Li NMR experiments indicate that the minor component (the one having least intense signals) corresponds to a structure with $\{Li–OH_2\}^+$ encapsulated units, while the major component (that with the most intense signals) has no encapsulated lithium and/or water units, *i.e.* void. The remaining signals at 182.58 and 169.4 ppm are associated with residual amounts of the sodium salt structure (see above).[45] Interestingly the ^{1}H NMR spectra of an aged solution (6-8 days, room temperature) of this sample shows practically no signal associated to the species containing encapsulated $\{Li–OH_2\}^+$ units, thus indicating that the void structure is formed on prolonged standing.[57] No further attempts to obtain a pure sample of encapsulating $\{Li–OH_2\}^+$ cube were pursued under these conditions, although an enriched and inert, lithium-containing cube was accomplished by cation-exchange chromatography, as indicated in the following section.

The major component of the mixture was isolated by further Sephadex G-25 size-exclusion column chromatography, discarding the head and tail of the band. The ^{7}Li NMR spectrum of this eluate shows only the signal of solvated lithium cations thus indicating that the major component of the mixture effectively corresponds to the void architecture; its ^{13}C NMR also indicates the distinct uniqueness of the species (Figure S1a). In this respect, the lithium to sodium exchange of this fraction, conducted by DEAE

A-25 Sephadex anion exchange chromatography, produced a sample with no lithium ions (as shown by ICP analysis). ICP metal analysis of this compound allowed the comparison of the UV-Vis spectra of the structures prepared (Figure 3a). The sample of the major component (*i.e.* void) thus obtained was characterised by cyclic voltammetry experiments (Figure 3b). Four consecutive reversible $Fe^{III/II}$ responses are apparent in the $\{Fe^{II}(CN)_6\}$ oxidation zone, indicating that the structure is rather similar to that reported for the potassium salt (no encapsulated water). The CV shows some signals (see below and reference [45]) from the presence of residual sodium ions in the building block materials (as seen in the ^1H NMR spectrum, Figure S1b).

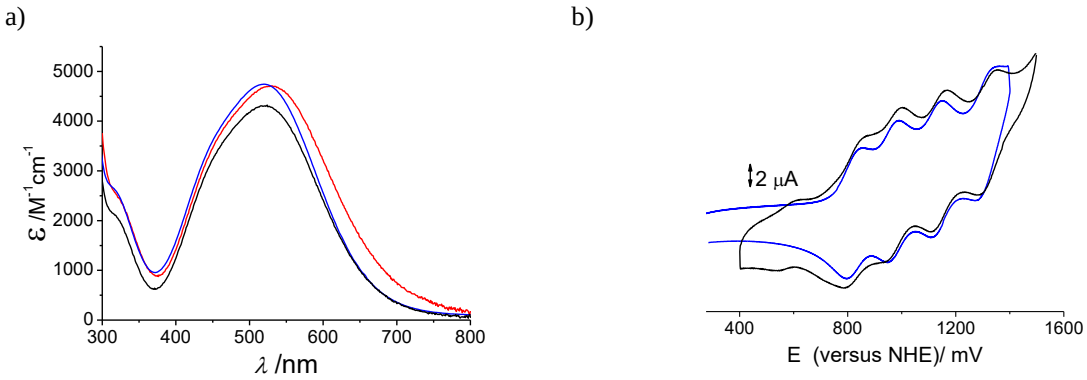

Figure 3.- a) Electronic spectra of the major component (*i.e.* void) of the lithium (black), sodium (red) and potassium (blue) salts of the $[\{Co^{III}(Me_3\text{-tacn})\}_4\{Fe^{II}(CN)_6\}_4]^{4-}$ species in water; b) Cyclic voltammograms of the Fe^{III}/Fe^{II} region of the major component of the lithium salt (*i.e.* void) (black, the minor signal at *ca.* 500 mV is associated to residual sodium salt of the species) and potassium salt (blue) of the $[\{Co^{III}(Me_3\text{-tacn})\}_4\{Fe^{II}(CN)_6\}_4]^{4-}$ cubic cage.

Summarising, the major kinetic product obtained using $Li_4[Fe^{II}(CN)_6]$ as $\{Fe^{II}(CN)_6\}$ building block has $\{Li–OH_2\}^+$ encapsulated units that leach from the cube into the bulk solution on workup and long standing, producing a thermodynamically stable void cubic $\{\{Co^{III}(Me_3\text{-tacn})\}_4\{Fe^{II}(CN)_6\}_4\}$ structure. Even so, the enrichment of a sample of $\{\{Co^{III}(Me_3\text{-tacn})\}_4\{Fe^{II}(CN)_6\}_4\}$ containing $\{Li–OH_2\}^+$ units was achieved by cation-exchange on DEAE A-25 Sephadex resin (see Adsorption cation-exchange study section), and a full characterization of the $\{\{Li–OH_2\}\subset[\{Co^{III}(Me_3\text{-tacn})\}_4\{Fe^{II}(CN)_6\}_4]\}$ was thus accomplished. Figure 4 displays the X-ray crystal structure of the cube $Li_8\{\{Li–OH_2\}\subset[\{Co^{III}(Me_3\text{-tacn})\}_4\{Fe^{II}(CN)_6\}_4]\}\cdot(ClO_4)_5\cdot 12H_2O$ compound, which is in agreement with the spectroscopic characterisation data available.

A very similar structure was determined for this complex *via* DFT calculations. The results from these produce a compound where the Li atom interacts with three nitrogen atoms of the bridging CN groups (average Li–N distance = 2.18 Å) and the water molecule occupies the centre of the cavity. This water molecule also shows four hydrogen bond interactions with different cyanido bridging ligands (average H…N distance = 2.55 Å). Interestingly, other species containing a lithium cation *plus* two or no water molecules were also computed producing compounds with higher Gibbs energies (13.6 and 25.4 kcal mol^{-1}, respectively), in excellent agreement with the experimental characterization of the complex encapsulating a $\{Li–OH_2\}^+$ unit. The hypothetical complex containing a $\{Li_2OH_2\}^{2+}$ unit was also computed, but found to be 10.2 kcal mol^{-1} higher in Gibbs energy.

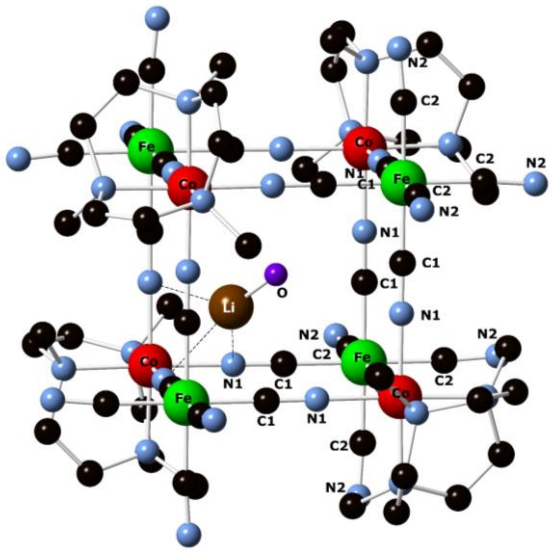

Figure 4.- Ball and stick representation of the cubic {{Li–OH_2}⊂[{Co^{III}(Me_3-tacn)}$_4${Fe^{II}($CN)_6$}$_4$]} structure of the Li_8{{Li–OH_2}⊂[{Co^{III}(Me_3-tacn)}$_4${Fe^{II}($CN)_6$}$_4$]}·$(ClO_4)_5$·12H_2O compound showing the encapsulated {Li–OH_2}.

Figure 5 shows the relevant maximum portal and cavity sizes of the cube, where the radius of C (0.60 Å) and N (0.54 Å) atoms of the cyanide groups have been taken from the literature data.[58] The values indicate that a sphere of a maximum radius of ~2 Å could be simplistically made to go through the square portal of the cube, and one of ~4 Å would fit inside the cubic cage. Figure 6 collects the comparison between the UV-Vis spectrum and cyclic voltammogram of the void and {Li–OH_2}$^+$-containing compounds prepared, showing clear differences between samples with and without inert water confined. It is interesting to note that on repetitive scanning the CV of the {Li–OH_2}$^+$-containing lithium salt cage evolves to that of the void cube (Figure 3a), thus indicating that the oxidation of the structure effectively labilises the {Li–OH_2}$^+$ units.

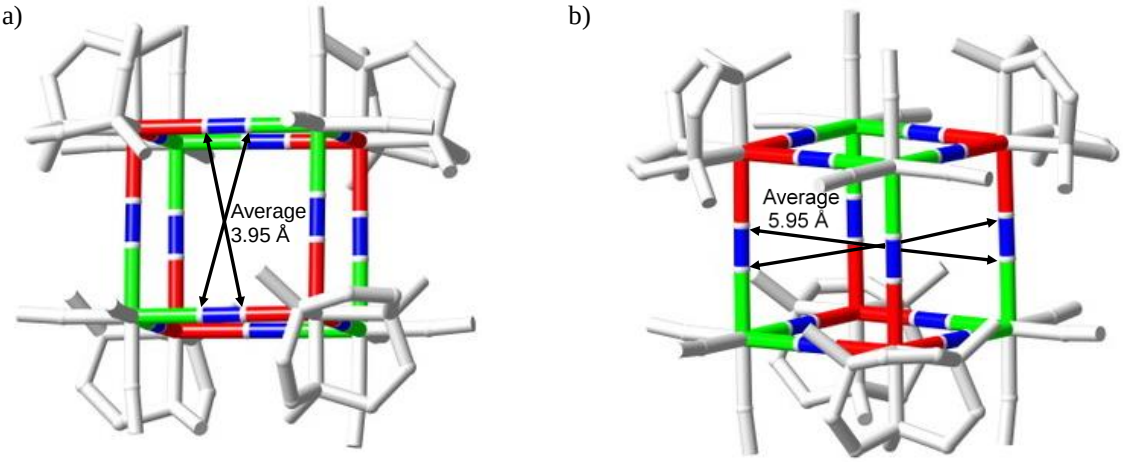

Figure 5.- Relevant portal (a) and cavity (b) dimensions of the cubic cage of the Li_8{{$LiOH_2$}⊂[{Co^{III}(Me_3-tacn)}$_4${Fe^{II}($CN)_6$}$_4$]}·$(ClO_4)_5$·12H_2O compound.

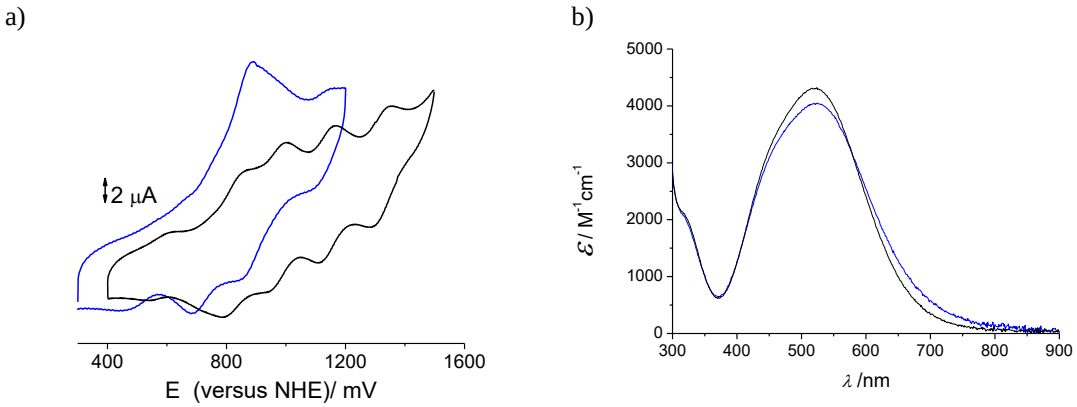

Figure 6.- a) Cyclic voltammograms of the Fe^{III}/Fe^{II} signals of the void (black) and $\{Li–OH_2\}^+$-containing (blue) lithium salts of the $[\{Co^{III}(Me_3\text{-tacn})\}_4\{Fe^{II}(CN)_6\}_4]^{4-}$ cubic cages; b) electronic spectra of the same samples.

Sodium salt

The general procedure for the preparation of the sodium salt of the $[\{Co^{III}(Me_3\text{-tacn})\}_4\{Fe^{II}(CN)_6\}_4]^{4-}$ complex has already been described, as well as its characterization by ^1H and ^{13}C NMR, UV-Vis, IR and ICP-OES spectroscopies, ESI-MS spectrometry and electrochemistry.[45]

As the solid compound always contains variable amounts of sodium perchlorate (arising from the anionic column chromatography workup), a purification procedure was conducted taking advantage of the robustness of the compound at diverse pHs. A dissolved sample of the compound was treated with concentrated HCl up to 5 M, which lead to the precipitation of the protonated neutral compound,[44-45] and the off-brown solid obtained was dissolved in 0.05 M NaOH after centrifugation. Slow evaporation of the solution in air, which slowly concentrates to pH 13-14, produced crystals of XRD quality that were subsequently analysed as $Na_3\{\{Na–OH_2\}\subset[\{Co^{III}(Me_3\text{-tacn})\}_4\{Fe^{II}(CN)_6\}_4]\}\cdot 22H_2O$. Figure 7 displays the cubic $[\{Co^{III}(Me_3\text{-tacn})\}_4\{Fe^{II}(CN)_6\}_4]^{4-}$ structure with the encapsulated $\{Na–OH_2\}^+$ unit which is disordered within the cube. Although the quality of the crystals obtained, their high symmetry and the large number of atoms and disordered water molecules involved do not allow for an ideal XRD analysis of the full structure, the confined $\{Na–OH_2\}^+$ unit is well resolved, which validates the relevant chemistry involved. In contrast to the $\{Li–OH_2\}^+$ analogue (Figure 4), where the cation occupies one corner of the cube contacting three N-atoms of bridging CN^- ligands and adopts a distorted tetrahedral geometry, the larger Na^+ ion on a face of the cube and makes four weak contacts with the cyanide N-atoms to adopt a square pyramidal coordination geometry with its axially coordinated aqua ligand.

This structure has also been proved with DFT calculations. In the calculated compound the sodium is close to one of the inner faces of the cubic structure, interacting with the nitrogens of four CN^- bridging ligands (average distance = 2.70 Å). The water molecule occupies the centre of the cavity and interacts with the nitrogen of two CN^- groups (average distance = 2.24 Å). The DFT calculations performed agree with the encapsulation of a single $\{Na–OH_2\}^+$ moiety; structures containing a sodium cation and two or no water molecules were found at higher Gibbs energies (19.2 and 15.5 kcal mol^{-1}, respectively). The

encapsulation of a dinuclear $\{Na_2OH_2\}^{2+}$ unit into the cubic cavity also produces a less stable complex (+7.0 kcal mol^{-1}).

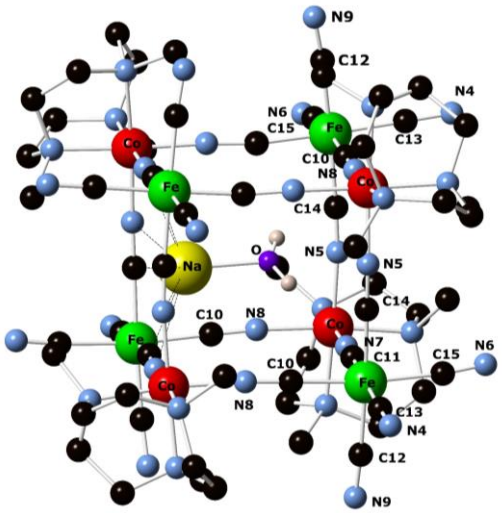

Figure 7.- Ball and stick representation of the cubic $\{\{Na–OH_2\}\subset[\{Co^{III}(Me_3\text{-tacn})\}_4\{Fe^{II}(CN)_6\}_4\}$ structure of the $Na_3\{\{Na–OH_2\}\subset[\{Co^{III}(Me_3\text{-tacn})\}_4\{Fe^{II}(CN)_6\}_4]\}\cdot 22H_2O$ compound showing the encapsulated $\{Na–OH_2\}$.

The relevant maximum dimensions for the square portal and cavity are also indicated in Figure 8, where the radius of C (0.60 Å) and N (0.54 Å) atoms have been used, as indicated above. Likewise, for the structure of the lithium counterpart, a sphere of a maximum radius of ~2 Å could go through the square portal of the cube, and one of ~4 Å could be set inside.

a) b)

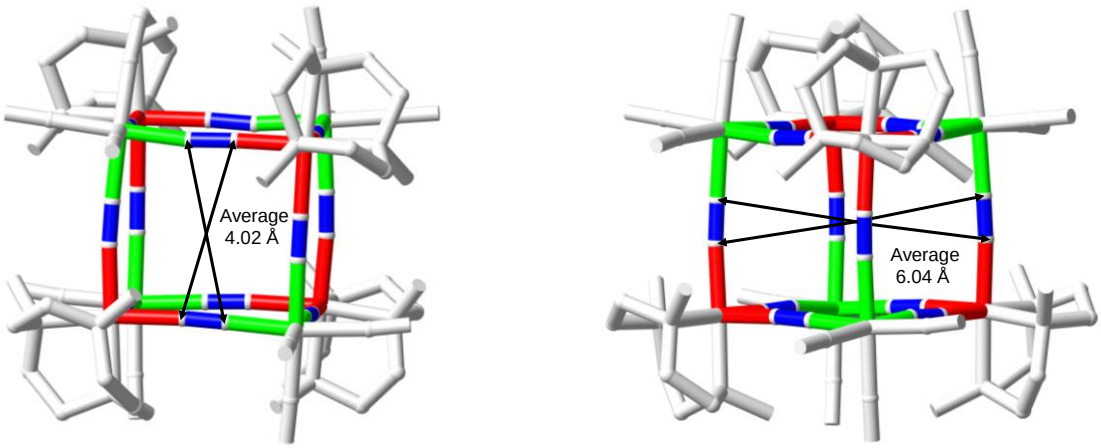

Figure 8.- Relevant portal (a) and cavity (b) dimensions of the cubic cage of the $Na_3\{\{Na–OH_2\}\subset[\{Co^{III}(Me_3\text{-tacn})\}_4\{Fe^{II}(CN)_6\}_4]\}\cdot 22H_2O$ compound.

The ^{1}H and ^{23}Na NMR spectra of these crystals in D_2O confirm the formulation established by the XRD studies, as well as the inert character of the sodium ion and water molecule confined inside the cubic cage. It should be noted (Figure 9) that the ^{23}Na NMR spectrum shows a broad signal for the ^{23}Na nucleus of the confined unit. This is expected from the value of its quadrupole moment, its non-cubic symmetry, and its likely fast tumbling inside the $\{\{Co^{III}(Me_3\text{-tacn})\}_4\{Fe^{II}(CN)_6\}_4\}$ cage (producing a sharp ^{1}H NMR resonance for the $\{Na–OH_2\}^+$ unit at 3.87 ppm).

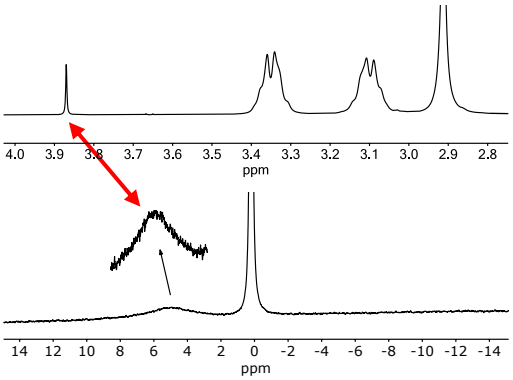

Figure 9.- ^{1}H (top) and ^{23}Na (bottom) NMR spectra of the $Na_3\{\{Na–OH_2\}\subset[\{Co^{III}(Me_3\text{-tacn})\}_4\{Fe^{II}(CN)_6\}_4]\}\cdot 22H_2O$ crystals dissolved in D_2O.

Potassium salt

The general procedure for the preparation and characterisation of the potassium salt of the $[\{Co^{III}(Me_3\text{-tacn})\}_4\{Fe^{II}(CN)_6\}_4]^{4-}$ complex has already been described.[45] The compound was found prevalent on the manipulation of the sodium salt samples, as expected from the exchange processes indicated in the next section. This prevalence (specially in ESI-MS procedures) is due to the unavoidable presence of potassium ions at micromolar concentration levels, as those used for manipulating of the complexes.[59] This fact precluded the use of HRMS-ESI as a reliable characterisation technique of the compounds described in this work.

The absence of a water molecule inside the cubic cavity is confirmed by DFT calculations. In this case the species encapsulating a simple K^+ cation is more than 15 kcal mol^{-1} lower in Gibbs energy than the structure with an encapsulated $\{K–OH_2\}^+$ unit. This fact also indicates that larger alkali metal cations *i.e.* Rb^+ and Cs^+, if encapsulated, would produce structures with the metal alone within the cubic structure.

Rubidium salt

The corresponding Rb^+ salt was obtained *in situ* by solution cation exchange (50-100 fold excess in order to have reasonable exchange times, see next section) of the sodium salt. The final exchanged solution was subsequently characterised by NMR, electrochemistry, ICP-OES, and UV-Vis spectroscopy (Figure S2). The absence of any encapsulated water in the cube is confirmed, as found for the potassium salt, by the absence of signals in the 3.5-4.5 region of the ^{1}H NMR spectrum; no differences were obtained when the spectrum was collected in 0.1 M RbCl solution. Figure 10 collects the changes observed in the aqueous

solution of the $Na_3\{\{Na–OH_2\}\subset[\{Co^{III}(Me_3\text{-tacn})\}_4\{Fe^{II}(CN)_6\}_4]\}\cdot 22H_2O$ compound after 24 h by electrochemistry, and ^1H and ^{23}Na NMR.

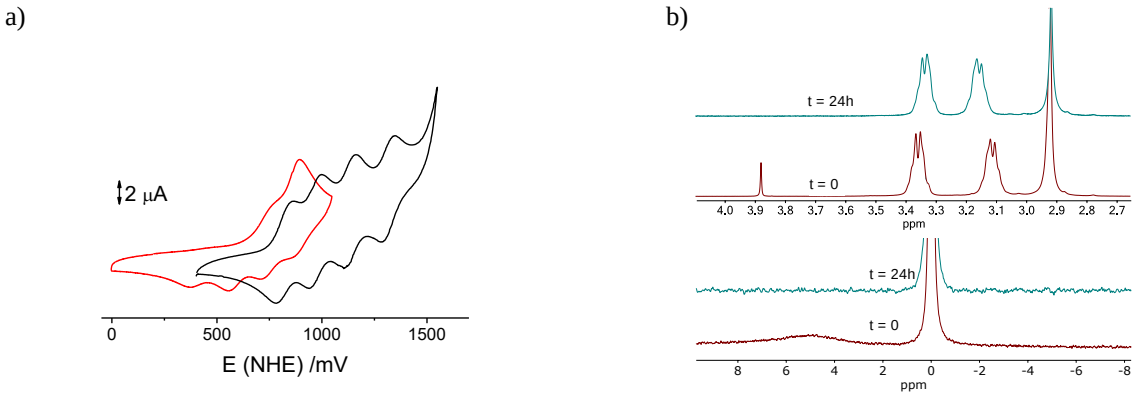

Figure 10.- a) Changes in the cyclic voltammogram of a 1×10^{-3} M solution of the sodium salt of the $[\{Co^{III}(Me_3\text{-tacn})\}_4\{Fe^{II}(CN)_6\}_4]^{4-}$ cube (red,[45]) in 0.20 M RbCl solution after 24 h (black). b) Changes in the ^1H (top) and ^{23}Na (bottom) NMR spectra of the same species at 1×10^{-2} M in 1.0 M RbCl.

When the sample was cation-exchanged by Sephadex DEAE A-25 anionic chromatography, in order to eliminate all 'external' rubidium cations *via* 0.25 M LiCl elution, the ICP-OES metal analysis indicated the absence of rubidium in the sample. Furthermore, the UV-Vis spectrum obtained after this chromatographic procedure corresponds to the cubic structure referred to as void in the synthesis of the lithium derivative (see Figure 2 and S2). That is, on anionic Sephadex DEAE A-25 chromatography the confined rubidium cations are eliminated on workup (see Adsorption cation-exchange study section).

Caesium salt

The preparation of the caesium salt of the $[\{Co^{III}(Me_3\text{-tacn})\}_4\{Fe^{II}(CN)_6\}_4]^{4-}$ cubic structure was tried *in situ* using the methodology indicated for the rubidium salt (see above). The process proved that, even after two weeks, the signals of 'confined' water and sodium in the ^1H and ^{23}Na NMR spectra do not diminish their intensity; the substitution by caesium of the $\{Na–OH_2\}^+$ unit is thus not occurring.

Solution cation-exchange kinetico–mechanistic study

In view of the important differences observed (with respect to the confinement and exchange of alkali cations and water in its cavity) in the behaviour of the cubic $\{\{Co^{III}(Me_3\text{-tacn})\}_4\{Fe^{II}(CN)_6\}_4\}$ structures prepared, we decided to study from a kinetico-mechanistic perspective the exchange processes at variable concentrations, ionic strength, temperature and pressure. In our previous report,[45] we had already shown that a K^+ for $\{Na–OH_2\}^+$ exchange study is feasible due to significant and reliable UV-Vis spectral changes. All processes involved with the species prepared, as seen in Figures 3b and S2b, are observed to quite sensitive spectroscopic UV-Vis changes. Interestingly, although the confined sodium to potassium and to rubidium exchange has been observed in an irreversible way, the known $\{\{K\}\subset[\{Co^{III}(Me_3\text{-tacn})\}_4\{Fe^{II}(CN)_6\}_4]\}$ cage[45] has not been observed to undergo the exchange to a rubidium species. Furthermore, the sodium to lithium exchange has not been observed, with prevalence in the ^1H NMR of the signal of the $\{Na–OH_2\}^+$ units upon solution (D_2O) of the sample in 0.1 M LiCl.

The preliminary results obtained for the {{Na–OH_2}⊂[{Co^{III}(Me_3-tacn)}$_4${Fe^{II}($CN)_6$}$_4$]} to {{K}⊂[{Co^{III}(Me_3-tacn)}$_4${Fe^{II}($CN)_6$}$_4$]} exchange process have been extended to different conditions of temperature, pressure and ionic strength to achieve the comprehensiveness of the studies. As already indicated,[45] the exchange process is not in equilibrium under pseudo-first order (excess entering cation) conditions. Furthermore, solution of the {{K}⊂[{Co^{III}(Me_3-tacn)}$_4${Fe^{II}($CN)_6$}$_4$]} species in 0.5 M NaCl does not produce any differences in the electronic spectrum, thus indicating the irreversibility of the exchange. The observed rate constants obtained for the exchange reaction are found independent of the entering cation concentration, at high concentration levels (0.050-0.10 M KCl) or low ionic strengths, as seen in Figure 11, which shows the effects observed on the values of k_{obs} on varying the value of [K^+] and I ([Na^+]). The data fit with a standard Eigen-Wilkins mechanism (Scheme S1) and rate law of the type indicated in Equation 1a,[60-62] with $K_{OS(K,Na)}$ corresponding to a mixed outer-sphere interaction of the alkaline cations with the anionic cubic structure.

$$k_{obs} = \frac{^{lim}k K_{OS(K,Na)}[\mathrm{K^+}]}{1 + K_{OS(K,Na)}[\mathrm{K^+}]} \qquad (1a)$$

$$= \frac{^{lim}k K_{OS(K)}[\mathrm{K^+}]}{1 + K_{OS(K)}[\mathrm{K^+}]} \quad \text{when } [\mathrm{Na^+}] = 0 \qquad (1b)$$

For the experiments run in the absence of any other added cations (experiments having a neat $K_{OS(K)}$ equilibrium constant, Equation 1b), the outer-sphere interactions are very large leading to $k_{obs} = {}^{lim}k$, and favouring a limiting exchange process.[61] From these limiting values of k_{obs} (*i.e.* those measured at [KCl] =0.10-0.20 M with no ionic strength added, according to Figure 11a) at different temperatures and pressures the corresponding thermal and pressure active activation parameters can be obtained using the standard Eyring (Figure 11b, top) or ln*k versus P* plots (Figure 11b, bottom).

It is clear that, as the $K_{OS(K,Na)}$ equilibrium constant is only apparent at high [Na^+] levels (and low [K^+] values), the mixed outer-sphere species slows-down the exchange.[63-64] This effect could be simplistically associated to the presence of dead-end outer-sphere interactions with the Na^+ cations, producing an alternative approximate rate law as that indicated in Equation 2a.

$$k_{obs} = \frac{^{lim}k K_{OS(K)}[\mathrm{K^+}]}{1 + K_{OS(K)}[\mathrm{K^+}] + K_{OS(Na)}[\mathrm{Na^+}]} \qquad (2a)$$

$$k_{obs} \approx \frac{^{lim}k[\mathrm{K^+}]}{[\mathrm{K^+}] + \frac{K_{OS(Na)}}{K_{OS(K)}}[\mathrm{Na^+}]} \qquad (2b)$$

Equation 2b is a simplification of Equation 2a for 1 << ($K_{OS(K)}$[K^+] + $K_{OS(Na)}$[Na^+]), which applies in our case, enabling thus the determination of a simplistic ($K_{OS(Na)}/K_{OS(K)}$) ratio at a given [K^+] and varying

[Na^+] values (Figure 12b, bottom). This value represents a measure of the productiveness of the outer-sphere precursor at different [Na^+] values; its value is also collected in Table 1 together with the relevant kinetic and activation parameters for the process.

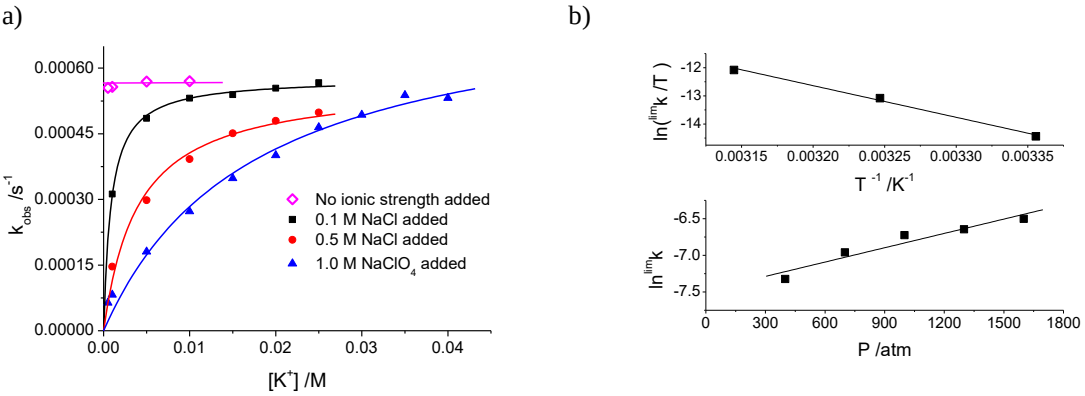

Figure 11.- a) [K^+]-dependence at 35 ºC in aqueous solution of the values of k_{obs} for the exchange from the sodium salt of the [{Co^{III}(Me_3-tacn)}$_4${Fe^{II}($CN)_6$}$_4$]$^{4-}$ cubic cages. b) Standard Eyring (top) or ln*k versus P* (bottom) plots for the changes of the value of ^{lim}k for the sodium-to-potassium cation exchange process with temperature and pressure.

Table 1.- Relevant kinetic and thermal and pressure activation parameters for the exchange reactions of the alkaline cations studied on the [{Co^{III}(Me_3-tacn)}$_4${Fe^{II}($CN)_6$}$_4$]$^{4-}$ cubic cages.

Exchange	Medium	$^{app}(K_{OS(medium)}/K_{OS(entering)})$	$10^4\times{}^{lim}k$ /s^{-1} (298 K)	$\Delta H^{\ddagger}$ /kJ mol^{-1}	$\Delta S^{\ddagger}$ /J $K^{-1}mol^{-1}$	$\Delta V^{\ddagger}$ /cm^3mol^{-1}
{Na–OH_2}$^+$ to K^+	0.10-1.0 M [Na^+]	$K_{OS(Na)}/K_{OS(K)}$ = 0.10 at 0.05 M [KCl]	1.7	94±7	-4±22	-16±3
	0.10 M [H^+]	$K_{OS(K)}$ = 40 M^{-1} in these conditions	190	51±4	-109±13	[a] ---
{Na–OH_2}$^+$ to Rb^+	0.010-0.10 M [Na^+]	$K_{OS(Na)}/K_{OS(Rb)}$ = 50 at 0.15 M [RbCl]	2.7	75±3	-64±10	-22±3
{Li–OH_2}$^+$ to {Na–OH_2}$^+$	0.0050-0.50 M [Na^+]	$K_{OS(Li)}$ = 30 M^{-1} at 0.050 M [NaCl]	0.63	64±4	-113±13	2.7±0.6
{Li–OH_2}$^+$ to K^+	0.050-1.0 M [Li^+]	[b] ≈ 0	0.33	93±9	-21±24	-16±1
{Li–OH_2}$^+$ to Rb^+	0.050-0.10 M [Li^+]	[b] ≈ 0	0.45	75±5	-79±15	-18±2
{Li–OH_2}$^+$ to void	----	not applicable	0.032	92±5	-44±15	-26±5

[a]: Not determined due to low solubility.
[b]: No dead-end ion-pair effect observed.

Given the fact that the {{Na–OH_2}⊂[{Co^{III}(Me_3-tacn)}$_4${Fe^{II}($CN)_6$}$_4$]} unit shows a well-established multiprotonation process with pK_a values of 2.3, 1.8, 0.93,[45] and that outer-sphere interaction of the alkali cations with the anionic cubic structure seems to be dominant, the {Na–OH_2}$^+$ to K^+ exchange process was also followed at acidic medium. The acidity, nevertheless, had to be limited to 0.10 M HCl due to solubility issues (see previous section, and the intensity of the UV-Vis spectrum in Figure S3). Although the thermal activation parameters (collected in Table 1) were determined from the k_{obs} data at 0.10 M KCl (k_{obs} = ^{lim}k, according to Figure S3b), the activation volume could not be determined for the same solubility issues. Under these acidic conditions the cubic structure is expected to be in a mixture of its di- and mono-anionic (di- and tri-protonated) forms, thus reducing considerably the value of $K_{OS(K)}$, as observed in Figure S3b. Furthermore, the significant changes produced on protonation in the cubic cage also translate on a faster exchange process based on enthalpy reasons ($\Delta H^{\ddagger}$ being reduced to *ca.* half the value at pH 7) despite a less favourable entropy term.

The kinetico-mechanistic study of the cation interchange was further pursued by the Rb^+ for $\{Na–OH_2\}^+$ exchange reaction, which had already been used for the preparation *in situ* of the rubidium salt (see previous section). As for the K^+ for $\{Na–OH_2\}^+$ exchange, the reaction showed well-behaved UV-Vis spectral changes that allowed the determination of the corresponding rate constants under pseudo-first order conditions (Figure 12a). Furthermore, when the exchange experiments were conducted in the presence of varying concentrations of NaCl, again a definite slowing-down effect was observed. In fact, the exchange process becomes too slow to be measured at *ca.* $[NaCl]_{added}$ >10×[RbCl] (Figure 12b, top), being [NaCl] >150×[KCl] for the K^+ for $\{Na–OH_2\}^+$ exchange (Figure 12b bottom). Even so, the absorbance changes are independent of the amount of NaCl added, indicating that no equilibrium is established. It thus clear that the same competition between productive and dead-end outer-sphere complexes, determined for the K^+ for $\{Na–OH_2\}^+$ exchange, is taking place in this case.

The values of k_{obs}, determined under pseudo-first order conditions and in the absence of any NaCl added (see Table S1), are found independent of the [RbCl] within the 0.020-0.50 M range (at a 5×10^{-5} M concentration level of the cubic cage). These correspond to the ^{lim}k values indicated above (Equation 1b at high entering cation concentrations), and were used for the determination of the thermal and pressure activation parameters indicated in Table 1, (Figure S4). The values determined (Table 1), indicate that, although for this exchange the enthalpy demand diminishes with respect to that by potassium, the entropy demand increases considerably, as well as the contraction occurring on going to the transition state.

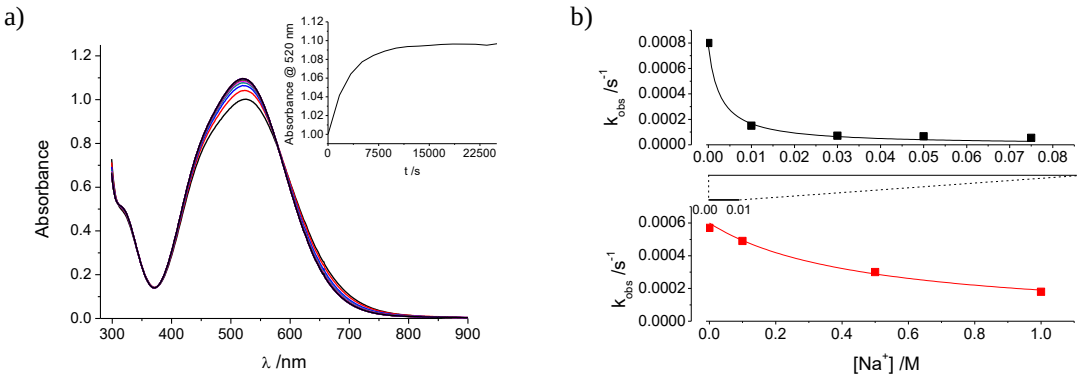

Figure 12.- a) UV-Vis spectral changes observed on the reaction of a 2×10^{-4} M aqueous solution of the sodium salt of the $[\{Co^{III}(Me_3\text{-tacn})\}_4\{Fe^{II}(CN)_6\}_4]^{4-}$ cubic cage with RbCl (0.15 M) at 25 ºC. b) Effect of the $[Na^+]$ added on the value of the observed rate constants for the confined cation exchange at $[[\{Co^{III}(Me_3\text{-tacn})\}_4\{Fe^{II}(CN)_6\}_4]^{4-}] = 1\times10^{-4}$ M; top: $\{NaOH_2\}^+$ to Rb^+ at 0.15 M [RbCl] (33 ºC); bottom: $\{NaOH_2\}^+$ to K^+ at 0.005 M [KCl] (35 ºC); note the ten-fold difference in the $[Na^+]$ concentration scale.

When the same exchange experiments were carried out on the major component obtained on the preparation of the lithium salt of the $[\{Co^{III}(Me_3\text{-tacn})\}_4\{Fe^{II}(CN)_6\}_4]^{4-}$ cage (*i.e.* void, see before), no reaction was observed with aqueous 0.25-0.50 M NaCl, KCl or RbCl solutions. The UV-Vis spectra remained unchanged for days despite the fact that significant intensity differences should be observed on cation entering, according to Figure 3b; no changes were observed in the ^1H NMR spectra either.

From that point, the study of the exchange of the $\{Li–OH_2\}^+$ units to other alkaline cations in the samples having been lithium-enriched by Sephadex DEAE A-25 chromatography of $\{\{Na–OH_2\}\subset[\{Co^{III}(Me_3\text{-}tacn)\}_4\{Fe^{II}(CN)_6\}_4]\}$ (see next section) was also conducted, for comparison with data for the $\{Na–OH_2\}^+$ unit-containing $[\{Co^{III}(Me_3\text{-}tacn)\}_4\{Fe^{II}(CN)_6\}_4]^{4-}$ cube. Experiments were run to monitor the loss of the encapsulated unit (*i.e.* from $\{Li–OH_2\}^+$ to void, as observed during the preparative procedures). Despite the small spectral changes (Figure S5a) the process could be followed by UV-Vis spectroscopy in a very reproducible way. From the variations of the values of k_{obs} *versus* temperature and pressure (Figure S5b) the values of the thermal and pressure activation parameters derived are collected in Table 1. The data agree very well with the ^{1}H NMR experiments, indicated in the previous section, and are within the values expected from the process, with solvation of the exiting lithium cation (ordering and compression) playing a crucial role, in this case not compensated by changes in the entering cation.

The reactions of the exchange of the cage having $\{Li–OH_2\}^+$ inert units (*i.e.* $\{\{Li–OH_2\}\subset[\{Co^{III}(Me_3\text{-}tacn)\}_4\{Fe^{II}(CN)_6\}_4]\}$) with K^+ or Rb^+ were also effective, as observed by UV-Vis and ^{1}H NMR spectroscopy (see Figure S6a for an example). Similarly to the $\{Na–OH_2\}^+$ exchange processes indicated before, the values derived for k_{obs} were found to be independent of the concentration of the entering cations in the 0.0050-0.10 M range (see Table S1), and no concentration-related differences in the absorbance changes were observed, in agreement with the lack of an equilibrium situation. The data at 0.10 M cation concentration have been used to determine the values of the activation parameters collected in Table 1 (see Figure S6b as an example). As already observed for the replacement of $\{Na–OH_2\}^+$ by K^+, the presence of Li^+ cations at different concentrations does not hamper the exchange (see Table S1) indicating that $K_{OS(K,\text{ or Rb})} >> K_{OS(Li)}$, thus changing Equation 2b to $k_{obs} \approx {}^{lim}k$. That is, ion-pairing with lithium cations does not behave as a dead-end phenomenon for these processes, in contrast with the fact observed when Na^+ was added to the $\{Na–OH_2\}^+$ exchange processes (see Table 1).

Interestingly the reaction of $\{\{Li–OH_2\}\subset[\{Co^{III}(Me_3\text{-}tacn)\}_4\{Fe^{II}(CN)_6\}_4]\}$ with NaCl showed distinct trends from those observed for the cations above:

i) ^{1}H NMR experiments at *ca.* 2×10^{-3} M concentration level (> 7×10^{-3} M in 'external' Li^+) showed a clear Li^+ to Na^+ exchange, while keeping the accompanying encapsulated non-deuterated water molecule from the $\{M–OH_2\}^+$ units inside the cage (see Figure 13a).

ii) Although no reaction is observed on solutions being *ca.* 5×10^{-5} M in $\{\{Li–OH_2\}\subset[\{Co^{III}(Me_3\text{-}tacn)\}_4\{Fe^{II}(CN)_6\}_4]\}$ cage (1.5×10^{-4} M in 'external' Li^+), a definite reaction is observed by UV-Vis spectroscopy at 2×10^{-4} M cage concentration levels (>7×10^{-4} M in 'external' Li^+).

iii) When the experiments at the 5×10^{-5} M cage concentration level were conducted with different concentrations of Li^+ (LiCl or $LiClO_4$), a definite reaction was observed by time resolved UV-Vis spectroscopy (see Figure 13b). The time span agrees with the ^{1}H NMR experiments, and the value of k_{obs} is found to decrease on decreasing the [LiCl] concentration (Figure S7).

In all cases, no equilibrium was observed, and the values of k_{obs} were found independent of the concentration of Na^+ or Li^+ cations provided the limiting behaviour indicated in Figure S7 is attained (see above). The results agree with an initial outer-sphere fast equilibrium reaction producing an $\{Li^+;\{Li–$

$OH_2\}\subset[\{Co^{III}(Me_3\text{-tacn})\}_4\{Fe^{II}(CN)_6\}_4]\}^{3-}\}$ complex that represents the active species undergoing the exchange process quantified by Equations 1 and 2, with $k_{obs} \approx {}^{lim}k$. In this case, contrary to its sodium counterpart, the outer-sphere complex of the cage is not a dead-end species, but instead the active species for the Li^+ to Na^+ exchange within the $\{M–OH_2\}^+$ units. The values of k_{obs} at [LiCl] = 0.050 M and [NaCl] = 0.10 M have been used for the derivation of the thermal and pressure activation parameters collected in Table 1. The value of the equilibrium constant leading to the formation of the active precursor species ($^{app}(K_{OS(medium)}/K_{OS(entering)})$) is also collected there, where it is made clear that important differences exist in the process involved. The values of enthalpy and entropy of activation are very distinct from the other exchange processes studied, with the exception of that on the protonated species of the $\{\{Na–OH_2\}\subset[\{Co^{III}(Me_3\text{-tacn})\}_4\{Fe^{II}(CN)_6\}_4]\}$ structure (a situation rather similar to that of a tight outer-sphere complex with a Li^+ cation). The sign of the value of the volume of activation is also reversed, indicating a small expansion on going to the transition state, contrarily to the rather homogeneous contraction observed for the other reactions shown in Table 1.

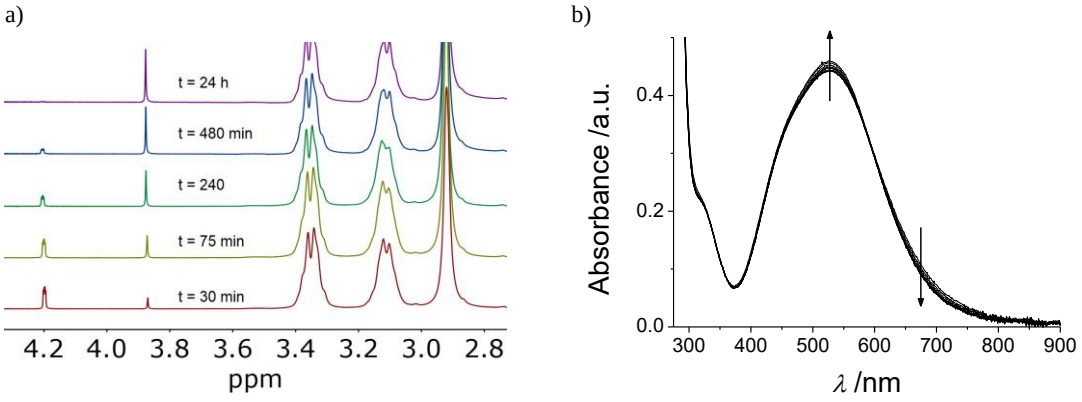

Figure 13.- a) Time-resolved ^1H NMR changes observed upon solution of a sample of $\{\{Li–OH_2\}\subset[\{Co^{III}(Me_3\text{-tacn})\}_4\{Fe^{II}(CN)_6\}_4]\}$species in 0.10 M NaCl. b) UV-Vis spectral changes observed for a 5×10^{-5} M sample of the same compound 0.10 M NaCl and 0.05 M LiCl at 35 ºC.

Adsorption cation-exchange study

As indicated in the preparative section, the $\{\{Rb\}\subset[\{Co^{III}(Me_3\text{-tacn})\}_4\{Fe^{II}(CN)_6\}_4]\}$ unit loses its encapsulated rubidium cation on chromatography exchange with Li^+ on Sephadex DEAE A-25, and consequently, the void cubic structure is obtained. In view of these results, we have conducted a comprehensive study on these heterogeneous processes occurring on the fully characterized lithium and sodium salts of the $[\{Co^{III}(Me_3\text{-tacn})\}_4\{Fe^{II}(CN)_6\}_4]^{4-}$ cubic cages.

On loading an aqueous solution of the $Na_3\{\{Na–OH_2\}\subset[\{Co^{III}(Me_3\text{-tacn})\}_4\{Fe^{II}(CN)_6\}_4]\}\cdot22H_2O$ complex on a Sephadex DEAE A-25 anion exchange column, a single very well defined and very narrow band is held on the top (as would be expected from its large negative charge). After thorough washing with water, elution was commenced with 0.1 M $NaClO_4$; the band started moving rather sluggishly and the concentration of the eluent was increased to 0.3 M. The purple solution thus obtained, was quickly taken to dryness at room temperature and thoroughly washed with acetone to eliminate most of the free

$NaClO_4$. The ^1H NMR spectrum of this sample shows the signal of the confined water molecule at 3.87 ppm with an intensity that is identical to that of the initial sample, indicating that under these conditions the $\{Na–OH_2\}^+$ units are not expelled from the cage.

When the same experiment was conducted by elution with $LiClO_4$, the final sample showed a ^1H NMR spectrum with a less intense signal at 3.87 ppm (from the confined $\{Na–OH_2\}^+$ units). Furthermore, the appearance of a quadruplet at 4.21 ppm indicated that encapsulated $\{Li–OH_2\}^+$ units were present, which is in absolute contradiction with the behaviour observed in homogenous aqueous solution. After a 10-fold dilution the loading/elution process was repeated 3 more consecutive times, and the $\{Na–OH_2\}^+$ to $\{Li–OH_2\}^+$ unit exchange is observed to have occurred up to 75 % (Figure 14a). The ^{13}C NMR spectrum is even more revealing when compared with that in Figure 2b, the signals of the sodium cage are practically not observed, while the signals of the void cubic structure are apparent due to the long acquisition times required for a reliable spectrum, during which some $\{Li–OH_2\}^+$ to void exchange occurred (see previous section). Enrichment of the sample by repeating the procedure indicated above 4 more times produced up to a 9:1 ratio of cages encapsulating either $\{Li–OH_2\}^+$ or $\{Na–OH_2\}^+$ units, respectively. From the final sample XRD-quality crystals were obtained and analysed (see Figure 4).

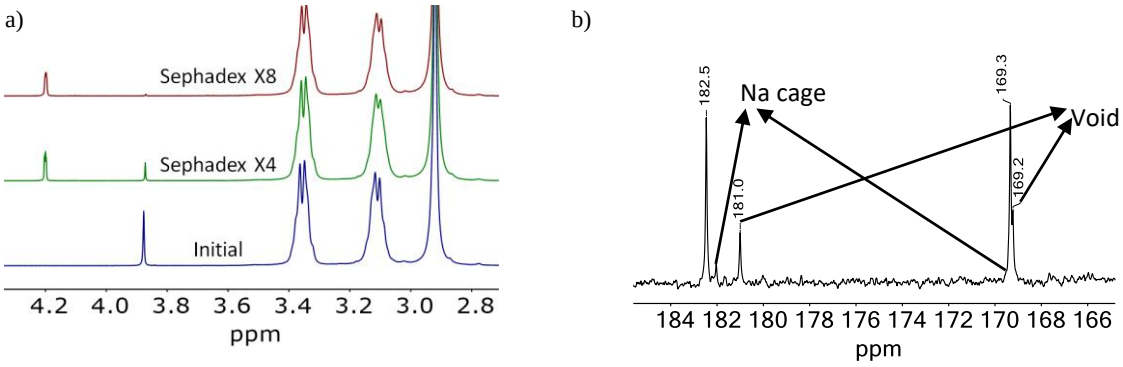

Figure 14.- a) ^1H NMR spectral changes observed after four and eight repetitions of a DEAE A-25 Sephadex $LiClO_4$-eluted chromatography of a sample of the sodium salt of the $[\{Co^{III}(Me_3\text{-tacn})\}_4\{Fe^{II}(CN)_6\}_4]^{4-}$ cubic cage (see text). b) ^{13}C NMR spectrum of the intermediate sample (Sephadex ×4).

The crude compound obtained from the preparation of the lithium salt of the $[\{Co^{III}(Me_3\text{-tacn})\}_4\{Fe^{II}(CN)_6\}_4]^{4-}$ cube was studied in a similar way. In this case, again the signal of the residual $\{Na–OH_2\}^+$ units present in the crude product disappear on $LiClO_4$ elution from a Sephadex DEAE A-25 column, while elution with $NaClO_4$ produces a solution without the signal of the encapsulated $\{Li–OH_2\}^+$ unit. It is not clear if this latter effect is due to the heterogeneous reaction on the adsorbed sample or to the simple 'emptying' of the lithium $\{Co^{III}(Me_3\text{-tacn})\}_4\{Fe^{II}(CN)_6\}_4\}$ cubic cage on standing, as indicated in the previous preparative and solution exchange sections.

Discussion

Compounds

The preparation and isolation of the lithium, sodium and potassium salts of the cube indicated in Chart 1 has been achieved by self-assembly of {Co^{III}-NC-Fe^{II}} edge units generated from the outer-sphere redox/labile substitution/inner-sphere redox processes known for some time and that we have comprehensively developed.[41, 55, 65] The presence of {Co^{III}-NC-Fe^{II}-CN-Co^{III}} units can also be achieved from the same processes, but the prevalence of *trans* isomerism of the Fe^{II}-hexacyanido unit would not permit the formation of a cubic structure, which requires a *fac* isomeric assembly.[42] In this respect, the formation of tetranuclear *mer*-{$(Co^{III}\text{-NC})_3$-Fe^{II}} assemblies has also been reported.[43] Nevertheless, its formation necessitates substitution processes on the inert Co^{III} centres, both due to the dramatic increase on the $E^0_{(Fe^{III}/Fe^{II})}$ redox potential, and the need of a $(2+)_{([Co^{III}\text{-NC-}Fe^{II}\text{-CN-}Co^{III}\})}/(3+)_{\{Co^{III}\}}$ outer-sphere contact.[43] The final self-assembly process from the {Co^{III}-NC-Fe^{II}} edge units is clearly evidenced by the absence of measurable amounts of any {$(Co^{III}\text{-NC})_2$-Fe^{II}} or {$Co^{III}(\text{-NC-}Fe^{II})_2$} species in solution, even when large excesses of iron or cobalt building block are used.[45] Clearly the final assembly process is driven by thermodynamics and the relatively less inert character of the ancillary monodentate ligands on the initial {$Co^{III}(Me_3\text{-tacn})$} building block unit.[66]

The characterisation of the compounds has been achieved using standard techniques. ^{7}Li and ^{23}Na NMR, and ^{1}H DOSY experiments also provided a clear evidence of the confined character of alkali metal ions and the associated slowly exchanging water molecule for the sodium and lithium species. Electrochemical experiments for the structures having a tumbling$\{M–OH_2\}^+$ unit inside show an irreversible behaviour, which is not present for the simpler void, K^+ and Rb^+-containing structures, where four fully reversible and independent iron-centred redox processes are observed as for other units of the same family of compounds.[44, 46-47, 52, 54, 67] Clearly, the distinct oxidation of the Fe^{II} units seems to be highly affected by the presence of dynamically distributed {M–OH_2} entities inside the cube. As for the XRD data, the bond distances are the expected according to all the data available. The Co^{III}-NC-Fe^{II} distance is within the 4.90-4.94 Å range observed for all the di- and trinuclear structures indicated in Chart 1, and slightly larger than that observed for the protonated {$(Co^{III})_2(\text{-NC-}Fe^{II})_2$} square structure (4.83 Å). The intermetallic distances are effectively shorter than the Fe^{III}-NC-Fe^{II} observed in PrussianBlue (5.07 Å)[68] as expected from the differences in the electronic nature between the Fe^{III} and Co^{III} centres.

It is also important to mention the preparative origin of the internal cage-encapsulated units (despite the substitution processes observed), in all cases the kinetically controlled assembled structures are generated by encapsulating the cations available in the assembly medium. The stability of the structure containing the $\{Na–OH_2\}^+$ units in comparison with that containing the equivalent $\{Li–OH_2\}^+$ entities is remarkable, as the sodium form is found even if only residual quantities of sodium are present in the reaction medium (see preparation of lithium salt). Furthermore, the structure with encapsulated $\{Li–OH_2\}^+$ units tends to lose its guest to the medium thus providing the void structure. In the same line, the surprising fact that the lithium inner cations are exchanged to sodium while maintaining the confined water[57] indicates the

structural stabilising importance of the encapsulated water molecule (already observed in the electrochemical experiments) for these small alkali metal cations.

The void cubic structure detected on dissociation of the $\{Li–OH_2\}^+$ units from the lithium-assembled species merits some discussion. The cavity size of the structures indicated in Figures 4 and 7 clearly shows that an empty possibility is not feasible. Although the possible existence of encapsulated water clusters inside of the cubic structure cannot be ruled out,[11, 69] the proton exchange with the deuterated D_2O solvent makes them undetectable by ^1H NMR. Nevertheless, the absence of any positive charge inside a highly negative cavity, would point to a labile exchange of any Lewis base such as water.

Aqueous cation exchange

With respect to the kinetico-mechanistic study of the exchange reactions in solution of the encapsulated units inside the $[\{Co^{III}(Me_3\text{-tacn})\}_4\{Fe^{II}(CN)_6\}_4]^{4-}$ cube, three general aspects have to be considered from the data in Table 1. *i*) The unobserved entry of alkaline cations inside the void cube. *ii*) The irreversible exchange sequence observed. *iii*) The determinant involvement of outer-sphere complexes in the processes.

On one hand, the exchange processes seem to be only thermodynamically favoured on hydration of cations contained inside the cage structure. That is, the entry of hydrated alkaline cationic entities into void cubes is not occurring, as it implies uncompensated dehydration of the entering units. Furthermore, in aqueous solution, only a one-way, from smaller to larger alkali metal cation is observed, indicating that the more favoured hydration of the exiting smaller encapsulated units in the cage plays a determining role. The substitution sequence does not operate starting from the potassium-containing cage, thus indicating the rather good energetic fitting of the cation inside the cage.

On the other hand, although outer-sphere ion-pairing between (4-) and (1+) charges in solution is expected (producing the observed limiting kinetics),[61, 70-71] the Na^+-dead-end and Li^+-activating selective pairing in the $\{Na–OH_2\}^+$ (to K^+ and Rb^+) and$\{Li–OH_2\}^+$ (to $\{Na–OH_2\}^+$) exchanges, is remarkable. Clearly the outer-sphere $\{Na^+;\{\{Na–OH_2\}^+ \subset[\{Co^{III}(Me_3\text{-tacn})\}_4\{Fe^{II}(CN)_6\}_4]^{4-}\}$ pairs are stable and comprehensive enough (see Table 1) to hamper the precursor pairing with K^+ or Rb^+ thus stopping the exchange process, the effect being more important with the larger Rb^+ species. For the $\{\{Li–OH_2\}^+ \subset[\{Co^{III}(Me_3\text{-tacn})\}_4\{Fe^{II}(CN)_6\}_4]^{4-}\}$ architecture the equivalent $\{Li^+;\{\{Li–OH_2\}^+ \subset[\{Co^{III}(Me_3\text{-tacn})\}_4\{Fe^{II}(CN)_6\}_4]^{4-}\}\}$ pairs do not only not hamper the reaction, activating the $\{Li–OH_2\}^+$ to $\{Na–OH_2\}^+$ exchanges instead. Clearly the nature of the precursor $\{Na^+;Li^+;\{\{Li–OH_2\}^+ \subset[\{Co^{III}(Me_3\text{-tacn})\}_4\{Fe^{II}(CN)_6\}_4]^{4-}\}\}$ does not correspond merely to a simple ion-pair complex. This is a fact that can be related with the small size of the lithium cation[72-73] that should parallel the behaviour of $\{Li^+;\{\{Li–OH_2\}^+ \subset[\{Co^{III}(Me_3\text{-tacn})\}_4\{Fe^{II}(CN)_6\}_4]^{4-}\}$ with the species obtained on protonation of the cubic structure (see below). Similarly, specific kinetic runs on the $\{Na–OH_2\}^+$ to K^+ exchange were carried out in the presence of high ionic strength concentrations (*ca.* 1-3 M) of $LiClO_4$. The rate constant values were about 1.5-2.0 fold higher than the values obtained for ^{lim}k when Na^+ or no ionic strength medium was

used (see Table S1). Undoubtedly, the effect of Li^+ association with the $\{\{Na–OH_2\}^+ \subset [\{Co^{III}(Me_3\text{-}tacn)\}_4\{Fe^{II}(CN)_6\}_4]^{4-}\}$ compound also activates the $\{Na–OH_2\}^+$ to K^+ exchange.

As for the kinetic and activation parameters collected in Table 1, they must be considered in groups, according to the discussion above. The simpler discussion correspond to the formation of the void structure from the $\{\{Li–OH_2\} \subset \{\{Co^{III}(Me_3\text{-}tacn)\}_4\{Fe^{II}(CN)_6\}_4\}\}$ architecture. The value of the rate constant at 25 ºC is one order of magnitude smaller than the rest of exchanges involving this species, while the values of the enthalpy and entropy of activation are rather similar to the exchange by K^+ and close to those by Rb^+. Interestingly, the value of the volume of activation is much more negative indicating the neat simple hydration of the existing $\{Li–OH_2\}^+$ units, thus compressing some of the external aqueous medium.

With respect to the $\{Li–OH_2\}^+$ to K^+ and Rb^+ exchange, the values of the rate constants are rather similar. The values of the thermal activation parameters show an $\Delta H^{\ddagger}(K^+) > \Delta H^{\ddagger}(Rb^+)$ and $\Delta S^{\ddagger}(K^+) > \Delta S^{\ddagger}(Rb^+)$ sequence, in accordance with a higher energetic and disorder demands for the dehydration and entry of the smaller K^+, when compared with the less well-hydrated entering Rb^+. The trend of the values of the activation volumes is in very good agreement with the entropy data. This reasoning parallels the trends arising from the exchange of $\{Li–OH_2\}^+$ by K^+ and Rb^+ on the $\{\{Li–OH_2\} \subset [\{Co^{III}(Me_3\text{-}tacn)\}_4\{Fe^{II}(CN)_6\}_4]\}$ non-protonated architecture. That is, the energetic signature of these reactions from simple ion-paired $\{\{M–OH_2\}^+ \subset [\{Co^{III}(Me_3\text{-}tacn)\}_4\{Fe^{II}(CN)_6\}_4]^{4-}\}$ structures is common to all the exchange processes.

The two remaining entries in Table 1 are associated to rather different reaction starting materials. The reaction correspond, either to the $\{Na–OH_2\}^+$ exchange on a partially protonated (*i.e.* $\{\{Na–OH_2\}^+ \subset [\{Co^{III}(Me_3\text{-}tacn)\}_4\{Fe^{II}(CN)_6\}_4H_{(2\text{ or }3)}]^{(2-\text{ or }-)}\}$),[45] or tightly bound ion-pairs (*i.e.* $\{Li^+;\{\{Li–OH_2\}^+ \subset [\{Co^{III}(Me_3\text{-}tacn)\}_4\{Fe^{II}(CN)_6\}_4]^{4-}\}\}$) architectures. In both cases the effective charge of the cubic cage should be considered less negative, which should enable a lower enthalpy demanding positive unit exiting process. In the same way, the values obtained for the activation entropy for these processes are more negative, indicating a higher ordered transition state, which is accompanied by a surprising small expansion for the $\{Li–OH_2\}^+$ to $\{Na–OH_2\}^+$ exchange. The combination of these two apparently opposite trends have been repetitively associated in a variety of reactions with the actuation of a hydrogen-bonding and ordered solvent network interactions in the transition state.[74-76] This fact agrees very well with the presence of positive charges (H^+ or Li^+) tightly bound to the $[\{Co^{III}(Me_3\text{-}tacn)\}_4\{Fe^{II}(CN)_6\}_4]^{4-}$ cubic cage.

Finally the aspects related to the$\{Na–OH_2\}^+$ by $\{Li–OH_2\}^+$ substitution on Sephadex DEAE A-25 chromatography have to be discussed in view of the formally thermodynamically uphill reaction in aqueous solution, where the inverse irreversible process is observed. The process observed results in extraction from the cage of $\{Na–OH_2\}^+$ units or Na^+ cations that are replaced by the smaller lithium counterparts, the final compound being the somehow elusive $\{Li–OH_2\}\subset[\{Co^{III}(Me_3\text{-}tacn)\}_4\{Fe^{II}(CN)_6\}_4]\}$ structure, obtained only as a minor product during preparative procedures. The

adsorption of the highly charged {{Na–OH_2}⊂[{$Co^{III}(Me_3$-tacn)}$_4${$Fe^{II}(CN)_6$}$_4$]} species on the protonated diethylaminoethyl positively charged bead results in expelling the encapsulated sodium. From that point, the smaller lithium cations enter the cubic cage adsorbed architecture (which is not observed in solution). The non-observed entry of the same species into the void {{$Co^{III}(Me_3$-tacn)}$_4${$Fe^{II}(CN)_6$}$_4$]} Sephadex-immobilised species can be directly related to a probable smaller size of the portal in such a complex as seen in the trends on Figures 5 and 8. A similar anchoring process on acidic surfaces has been observed for this type of complexes,[53] and more recently the expansion/compression of some helicoidal structures have been detected in solution/solid state, involving the expulsion of some encapsulated cations.[77]

Conclusions

The redox-triggered assembly reaction of cubic mixed-valence cyanide bridged Co^{III}/Fe^{II} compounds (PBAs) can be achieved using different alkali metal cations, that do not act innocently as counter cations of the highly negative units assembled. The complexes formed confined {M–OH_2}$^+$ or M^+ units in a rather inert manner, depending on the size of the metal ions involved, which makes the cubes hosts for these cation guests. The compound with an {Na–OH_2}$^+$ encapsulated unit is highly resistant in rather extreme acidic and basic aqueous media, but can be exchanged to that with a K^+ cation that seems to be the thermodynamic well of cation exchange processes. The equivalent complex with confined {Li–OH_2}$^+$ loses its guest to the bulk solution on prolonged standing producing a non-reactive void {$Co^{III}(Me_3$-tacn)}$_4${$Fe^{II}(CN)_6$}$_4$]} structure. Electrochemistry and ^{1}H NMR spectroscopy represent excellent tools for the distinction between confined {M–OH_2}$^+$ or M^+ units.

The non-innocent behaviour of the counter cations in the chemistry involved is also evident when exchange reactions of the confined cationic units are considered. Formation of ion-pair complexes between the highly negatively charged cubic units and Na^+ produce dead-end blocking of the exchange reactions while for Li^+ ion pairing the substitution process is accelerated as for partial protonation of the cubic species.

The ligand nature of the cages can be studied kinetico-mechanistically *via* the exchange processes of their different alkali metal salts. The processes show an energetic signature that involves the differences between the hydration of the entering and leaving cations, as differences in the entropy and volume of activation indicate. The strongly hydrogen bonded character of the water inside the cage is indicated both by its lower acidity (as seen by ^{1}H NMR) and the fact that the lithium to sodium exchange occurs while maintaining the same confined water (as seen by ^{1}H NMR in D_2O). The portal dimensions of the cage (as determined from XRD) also clearly explain the fact that no exchange to Cs^+ is observed in solution despite the persistent presence of encapsulated Cs^+ cations in PBAs.

The surprising uphill selective reaction from {{Na–OH_2}⊂[{$Co^{III}(Me_3$-tacn)}$_4${$Fe^{II}(CN)_6$}$_4$]} to {{Li–OH_2}⊂[{$Co^{III}(Me_3$-tacn)}$_4${$Fe^{II}(CN)_6$}$_4$]} (not occurring from void {{$Co^{III}(Me_3$-tacn)}$_4${$Fe^{II}(CN)_6$}$_4$]}) on samples adsorbed on DEAE A-25 Sephadex has to be explained by the immobilisation of an expanded {{Na–OH_2}⊂[{$Co^{III}(Me_3$-tacn)}$_4${$Fe^{II}(CN)_6$}$_4$]} species that allows the entry of a flooding amount of

Li^{+}_{aq} used for elution. This methodology opens up possibilities for the reversible entry of lithium cations in other structures.

Experimental

Physical Methods

^{1}H and ^{13}C NMR spectra were recorded on a Bruker-400Q or on a Bruker-500 spectrometers at 25 ºC at the Unitat de RMN d´Alt Camp de la Universitat de Barcelona, ^{23}Na and ^{7}Li NMR spectra were recorded on a Bruker-500 instrument. DOSY NMR measurements were performed on a Bruker 400 MHz NMR spectrometer (see supporting information).

ICP-OES and ICP-MAS was also carried out at the Centres Científics i Tecnològics (Universitat de Barcelona) on a Perkin Elmer Optima instrument. UV-Vis spectra were recorded on HP5483 or Cary50 instruments. IR spectra were recorded on a Thermo Scientific Nicolet iS5 FT-IR instrument using an ATR system.

Electrochemistry experiments were carried out at 25 ºC and at 100 mV s^{-1}, with a BioLogic SP-150 instrument. A glassy carbon working electrode, a Ag/AgCl (saturated KCl or NaCl) reference electrode and platinum wire counter electrode were used on 1×10^{-3} M solutions of the sample and using 0.1 M of the chloride (or perchlorate) cage cation concentration as supporting electrolyte. All potentials are given *versus* NHE, once corrected for the reference electrode used.

The kinetic profiles for the reactions at atmospheric pressure were followed by UV-Vis spectroscopy in the 900-300 nm range on a Cary50 or an Agilent HP8453A instrument equipped with thermostated multicell transports. For runs at elevated pressure, the previously described high-pressure set-up[74, 78-79] was used connected to a J&M TIDAS S300 instrument.

X-Ray Structure Analysis

For the lithium derivative of the cubic structure, a black prism-like specimen of $C_{60}H_{110}Cl_5Co_4Fe_4Li_9N_{36}O_{33}$, $Li_8\{\{LiOH_2\}\subset[\{Co^{III}(Me_3\text{-tacn})\}_4\{Fe^{II}(CN)_6\}_4]\}(ClO_4)_5\cdot12H_2O$, approximate dimensions 0.180×0.130×0.130 mm, was used for the XRD analysis. For the sodium derivative of the cubic structure, a black prism-like specimen of $C_{60}H_{130}Co_4Fe_4N_{36}Na_4O_{23}$, $Na_3\{\{NaOH_2\}\subset[\{Co^{III}(Me_3\text{-tacn})\}_4\{Fe^{II}(CN)_6\}_4]\}\cdot22H_2O$, approximate dimensions 0.180×0.270×0.460 mm, was used for the analysis. The X-ray intensity data were measured on a D8 Venture system equipped with a multilayer monochromator and a Mo microfocus (λ = 0.71073 Å) (see supporting information for details).

Materials

Compound $[Co(Me_3\text{-tacn})Cl_3]$ was prepared according to literature methods.[66] $Na_4[Fe^{II}(CN)_6]$ and $K_4[Fe^{II}(CN)_6]$ were recrystallized twice from the commercially available material before use. $Li_4[Fe^{II}(CN)_6]$ was prepared by a modification of the published procedure.[80] An aqueous solution of $K_4[Fe^{II}(CN)_6]$ was treated with an excess of a solution of $LiClO_4$ (3-fold), after cooling for 2-days at 3-4 ºC the resulting solution was filtered and taken to dryness at 50 ºC. The solid obtained was thoroughly washed with ethanol and the remaining off-white solid collected. IR spectrum $\nu_{(\text{stretch CN})}$= 2123, 2040 cm^{-1}

All the other commercially available chemicals were of analytical grade and were used as received.

Compounds

The preparation and isolation of all the different solid salts of the $[\{Co^{III}(Me_3\text{-tacn})\}_4\{Fe^{II}(CN)_6\}_4]^{4-}$ cube have been carried out by the same procedure, that has been already described.[45]

Briefly, to an 0.01 M aqueous suspension of $[Co(Me_3\text{-tacn})Cl_3]$ at pH 7-8 a 0.07 M solution of the corresponding salt of the $[Fe^{II}(CN)_6]^{4-}$ anion in a 2-3 fold excess (also at pH 7-8) was slowly added. The resulting mixture becomes very dark and, after left stirring overnight at 40-50 ºC, is filtered to eliminate any precipitated solids and loaded onto a Sephadex G-25 size exclusion chromatographic column (2×25 cm) in several aliquots. The retained dark band is eluted with water; an initial grey-blue polymer is discarded, while the central part of the remaining purple band was collected; a final trailing off-yellow band (excess of hexacyanidoferrate(II)) is also discarded. The procedure was repeated twice. After concentration to a small volume at 40-50 ºC, the remaining solution was left to evaporate to dryness in the air and the final solid sample was analysed by ICP (Fe:Co ratio), ^{1}H and ^{13}C NMR , ^{23}Na and ^{7}Li NMR (when applicable), UV-Vis and IR spectroscopy, and cyclic voltammetry. The characterization data for the sodium and potassium salt fully agree with those described[45] and are given in the supporting information together with that of the new salts prepared.

The lithium and sodium salts of the $[\{Co^{III}(Me_3\text{-tacn})\}_4\{Fe^{II}(CN)_6\}_4]^{4-}$ cage could also be purified by DEAE A-25 Sephadex chromatography. A solution of the prepared compounds (I = 0.05 M) is loaded onto the columns and eluted with 0.2-0.3 M $NaClO_4$ or $LiClO_4$. The eluted relevant was taken to dryness at room temperature, and the solid obtained thoroughly washed with acetone to eliminate the remaining sodium or potassium perchlorates. The alternative cross purification of the sodium salt by elution with $LiClO_4$ produced a lithium salt of the cage with distinct properties.

Computational details

All the density functional theory (DFT) calculations have been carried out using with the Gaussian09 (rev. D.01)[81] software. The hybrid functional PBE has been employed[82-83] for all the calculations along with def2svp[84-85] basis set for all the atom types. Ultrafine integration grids have been used in all calculations to ensure a satisfactory convergence. In all cases the solvation energies are computed in water with the (IEF-PCM) continuum dielectric solvation model[86-87] using the SMD radii and non-electrostatic terms.[88] The dispersion energy correction terms have been included by using the D3 method of Grimme.[89] Vibrational analyses have been performed for all the computed structures to ensure the nature of the stationary points, which have zero imaginary frequencies (see supporting information for details).

Acknowledgements

Financial support by Grant PID2019-107006GB-C21 funded by MCIN/AEI/ 10.13039/501100011033 is acknowledged.

Supporting Information

The Supporting Information is available free of charge at https://pubs.acs.org/doi/

Experimental details and characterisation procedures for the compounds prepared. NMR, UV-Vis and time resolved changes and k_{obs} trends for the reactions studied.

CCDC Accession Codes 2110263 and 2110264 contain the supplementary crystallographic data for this paper. These data can be obtained free of charge via www.ccdc.cam.ac.uk/data_request/cif, or by emailing data_request@ccdc.cam.ac.uk, or by contacting The Cambridge Crystallographic Data Centre, 12 Union Road, Cambridge CB2 1EZ, UK; fax: +44 1223 336033.

References

1. Robin, M. B.; Day, P., Mixed Valence Chemistry-A Survey and Classification. In *Advances in Inorganic Chemistry and Radiochemistry*, 10 ed.; Emeléus, H. J.; Sharpe, A. G., Eds. Academic Press: 1968; pp 247-422.
2. Marcus, R. A., Electron transfer reactions in Chemistry: Theory and experiment. *Angewandte Chemie International Edition* **1993,** *32*, 1111-1121.
3. Marcus, R. A., Chemical and electrochemical electron-transfer theory. *Annual Review of Physical Chemistry* **1964,** *15*, 155-196.
4. Taube, H., Electron transfer between metall compelxes. A retrospective view (Nobel Lecture). *Angewandte Chemie International Edition* **1984,** *23*, 329-340.
5. Brunschwig, B. S.; Creutz, C.; Sutin, N., Optical transitions of symmetrical mixed-valence systems in the class II-III transition regime. *Chemical Society Reviews* **2002,** *31*, 168-184.
6. Creutz, C., Mixed valence complexes of d^5-d^6 metall centres. *Progress in Inorganic Chemistry* **1983,** *30*, 1-73.
7. Barlow, K.; Johansson, J. O., Ultrafast photoinduced dynamics in Prussian blue analogues. *Physical Chemistry Chemical Physics* **2021,** *23*, 8118-8131.
8. Zimara, J.; Stevens, H.; Oswald, R.; Demeshko, S.; Dechert, S.; Mata, R. A.; Meyer, F.; Schwarzer, D., Time-Resolved Spectroscopy of Photoinduced Electron Transfer in Dinuclear and Tetranuclear Fe/Co Prussian Blue Analogues. *Inorganic Chemistry* **2021,** *60*, 449-459.
9. Ulusoy Ghobadi, T. G.; Ozbay, E.; Karadas, F., How to Build Prussian Blue Based Water Oxidation Catalytic Assemblies: Common Trends and Strategies. *Chemistry – A European Journal* **2021,** *27*, 3638-3649.
10. Ghobadi, T. G. U.; Ghobadi, A.; Demirtas, M., *et al.*, Building an Iron Chromophore Incorporating Prussian Blue Analogue for Photoelectrochemical Water Oxidation. *Chemistry – A European Journal* **2021,** *27*, 8966-8976.
11. Song, J.; Wang, L.; Lu, Y., *et al.*, Removal of Interstitial H_2O in Hexacyanometallates for a Superior Cathode of a Sodium-Ion Battery. *Journal of the American Chemical Society* **2015,** *137*, 2658-2664.
12. Aguila, D.; Prado, Y.; Koumousi, E. S.; Mathoniere, C.; Clerac, R., Switchable Fe/Co Prussian blue networks and molecular analogues. *Chemical Society Reviews* **2016,** *45*, 203-224.
13. Toma, L. M.; Lescouezec, R.; Lloret, F.; Julve, M.; Vaissermann, J.; Verdaguer, M., Cyanide bridged Fe(III)-Co(II) bis double zig-zag chgains with a slow relaxation of the magnetization. *Chemical Communications* **2003**, 1850-1851.
14. Jiménez, J.-R.; Glatz, J.; Benchohra, A.; Gontard, G.; Chamoreau, L.-M.; Meunier, J.-F.; Bousseksou, A.; Lescouëzec, R., Electron Transfer in the $Cs\subset\{Mn_4Fe_4\}$ Cubic Switch: A Soluble Molecular Model of the MnFe Prussian-Blue Analogues. *Angewandte Chemie International Edition* **2020,** *59*, 8089-8093.
15. Kamilya, S.; Ghosh, S.; Li, Y.; Dechambenoit, P.; Rouzières, M.; Lescouëzec, R.; Mehta, S.; Mondal, A., Two-Step Thermoinduced Metal-to-Metal Electron Transfer and ON/OFF Photoswitching in a Molecular $[Fe_2Co_2]$ Square Complex. *Inorganic Chemistry* **2020,** *59*, 11879-11888.
16. Cammarata, M.; Zerdane, S.; Balducci, L., *et al.*, Charge transfer driven by ultrafast spin transition in a CoFe Prussian blue analogue. *Nature Chemistry* **2021,** *13*, 10-14.

17. Wan, R.; Liu, Z.; Ma, X.; Li, H.; Ma, P.; Zhang, C.; Niu, J.; Wang, J., Discovery of two Na^{+}-centered Silverton-type polyoxometalates $\{NaM_{12}O_{42}\}$ (M = Mo, W). *Chemical Communications* **2021,** *57*, 2172-2175.
18. Garnier, D.; Jiménez, J. R.; Li, Y., *et al.*, $K\subset\{[Fe^{II}(Tp)(CN)_3]_4[Co^{III}(pzTp)]_3[Co^{II}(pzTp)]\}$: a neutral soluble model complex of photomagnetic Prussian blue analogues. *Chemical Science* **2016,** *7*, 4825-4831.
19. Hsu, S. C. N.; Ramesh, M.; Espenson, J. H.; Rauchfuss, T. B., Membership Rules for a Molecular Box: The Admission Process and Protection Provided to Guest Molecules. *Angewandte Chemie International Edition* **2003,** *42*, 2663-2666.
20. Jiménez, J. R.; Tricoire, M.; Garnier, D.; Chamoreau, L. M.; von Bardeleben, J.; Journaux, Y.; Li, Y.; Lescouëzec, R., A new $\{Fe_4Co_4\}$ soluble switchable nanomagnet encapsulating Cs^{+}: enhancing the stability and redox flexibility and tuning the photomagnetic effect. *Dalton Transactions* **2017,** *46*, 15549-15557.
21. Ludden, M. D.; Ward, M. D., Outside the box: quantifying interactions of anions with the exterior surface of a cationic coordination cage. *Dalton Transactions* **2021,** *50*, 2782-2791.
22. Ohara, E.; Soejima, T.; Ito, S., Removal of low concentration Cs(I) from water using Prussian blue. *Inorganica Chimica Acta* **2021,** *514*, 120029.
23. Saeed, S.; Boyd, S.; Tsai, W.-Y.; Wang, R.; Balke, N.; Augustyn, V., Understanding electrochemical cation insertion into prussian blue from electrode deformation and mass changes. *Chemical Communications* **2021,** *57*, 6744-6747.
24. Glatz, J.; Chamoreau, L.-M.; Flambard, A.; Meunier, J.-F.; Bousseksou, A.; Lescouëzec, R., Thermo- and electro-switchable $Cs\subset\{Fe_4–Fe_4\}$ cubic cage: spin-transition and electrochromism. *Chemical Communications* **2020,** *56*, 10950-10953.
25. Pedersen, C. J., The Discovery of Crown Ethers (Noble Lecture). *Angewandte Chemie International Edition* **1988,** *27*, 1021-1027.
26. Izatt, R. M.; Pawlak, K.; Bradshaw, J. S.; Bruening, R. L., Thermodynamic and Kinetic Data for Macrocycle Interaction with Cations, Anions, and Neutral Molecules. *Chemical Reviews* **1995,** *95*, 2529-2586.
27. Wang, X.; Cheng, L., Multifunctional Prussian blue-based nanomaterials: Preparation, modification, and theranostic applications. *Coordination Chemistry Reviews* **2020,** *419*, 213-393.
28. L. Heinrich, J.; A. Berseth, P.; R. Long, J., Molecular Prussian Blue analogues: synthesis and structure of cubic $Cr_4Co_4(CN)_{12}$ and $Co_8(CN)_{12}$ clusters. *Chemical Communications* **1998**, 1231-1232.
29. Nihei, M., Molecular Prussian Blue Analogues: From Bulk to Molecules and Low-dimensional Aggregates. *Chemistry Letters* **2020,** *49*, 1206-1215.
30. Siretanu, D.; Li, D.; Buisson, L.; Bassani, D. M.; Holmes, S. M.; Mathonière, C.; Clérac, R., Controlling Thermally Induced Electron Transfer in Cyano-Bridged Molecular Squares: From Solid State to Solution. *Chemistry – A European Journal* **2011,** *17*, 11704-11708.
31. Choudhury, A.; Pichon, C.; Sutter, J.-P.; Pamu, D.; Sarma, B.; Mudoi, P. P.; Gogoi, N., Accessing water processable cyanido bridged chiral heterobimetallic Co(ii)–Fe(iii) one dimensional network. *Chemical Communications* **2021,** *57*, 207-210.
32. Wei, X.; Wei, J.; Song, Y.; Wu, D.; Liu, X. D.; Chen, H.; Xiao, P.; Zhang, Y., Potassium mediated Co–Fe-based Prussian blue analogue architectures for aqueous potassium-ion storage. *Chemical Communications* **2021,** *57*, 7019-7022.
33. Northrop, B. H.; Zheng, Y.-R.; Chi, K.-W.; Stang, P. J., Self-Organization in Coordination-Driven Self-Assembly. *Accounts of Chemical Research* **2009,** *42*, 1554-1563.

34. Safont-Sempere, M. M.; Fernández, G.; Würthner, F., Self-Sorting Phenomena in Complex Supramolecular Systems. *Chemical Reviews* **2011,** *111*, 5784-5814.
35. Lorenz, Y.; Gutiérrez, A.; Ferrer, M.; Engeser, M., Bond Dissociation Energies of Metallo-supramolecular Building Blocks: Insight from Fragmentation of Selectively Self-Assembled Heterometallic Metallo-supramolecular Aggregates. *Inorganic Chemistry* **2018,** *57*, 7346-7354.
36. Angurell, I.; Ferrer, M.; Gutiérrez, A.; Martínez, M.; Rocamora, M.; Rodriguez, L.; Rossell, O.; Lorenz, Y.; Engeser, M., Kinetico-Mechanistic Insights on the Assembling Dynamics of Allyl Cornered Metallacycles; the Pt-Npy bond is the Keystone. *Chemistry – A European Journal* **2014,** *20*, 14473-14487.
37. Angurell, I.; Ferrer, M.; Gutiérrez, A.; Martínez, M.; Rodríguez, L.; Rossell, O.; Engeser, M., Antisymbiotic Self-Assembly and Dynamic Behavior of Metallamacrocycles with Allylic Corners. *Chemistry – A European Journal* **2010,** *16*, 13960-13964.
38. Ferrer, M.; Gallen, A.; Gutiérrez, A.; Martínez, M.; Ruiz, E.; Lorenz, Y.; Engeser, M., Self-Assembled, Highly Positively Charged, Allyl–Pd Crowns: Cavity-Pocket-Driven Interactions of Fluoroanions. *Chemistry – A European Journal* **2020,** *26*, 7847-7860.
39. Bernhardt, P. V.; Martínez, M., The First Structurally Characterized Discrete Dinuclear μ-Cyano Hexacyanoferrate Complex. *Inorganic Chemistry* **1999,** *38*, 424-425.
40. Bernhardt, P. V.; Bozoglián, F.; Macpherson, B. P.; Martínez, M., Tuning the metal to metal charge transfer energy of cyano-bridged dinuclear complexes. *Dalton Trans* **2004**, 2582-2587.
41. Bernhardt, P. V.; Bozoglián, F.; Macpherson, B. P.; Martínez, M., Molecular mixed-valence cyanide bridged Co^{III}-Fe^{II} complexes. *Coordination Chemistry Reviews* **2005,** *249*, 1902-1916.
42. Bernhardt, P. V.; Bozoglián, F.; González, G.; Martínez, M.; Macpherson, B. P.; Sienra, B., Dinuclear Cyano-Bridged Co^{III}/Fe^{II} Complexes as Precursors for Molecular Mixed Valence Complexes of Higher Nuclearity. *Inorganic Chemistry* **2006,** *45*, 74-82.
43. Bernhardt, P. V.; Martínez, M.; Rodríguez, C., Molecular Co^{III}/Fe^{II} Cyano-Bridged Mixed-Valence Compounds with High Nuclearities and Diversity of Co^{III} Coordination Environments: Preparative and Mechanistic Aspects. *Inorganic Chemistry* **2009,** *48*, 4787-4797.
44. Alcázar, L.; Bernhardt, P. V.; Ferrer, M.; Font-Bardia, M.; Gallen, A.; Jover, J.; Martínez, M.; Peters, J.; Zerk, T. J., Kineticomechanistic Study of the Redox pH Cycling Processes Occurring on a Robust Water-Soluble Cyanido-Bridged Mixed-Valence $\{Co^{III}/Fe^{II}\}_2$ Square. *Inorganic Chemistry* **2018,** *57*, 8465-8475.
45. Gonzálvez, M. A.; Gallen, A.; Ferrer, M.; Martínez, M., Self-Assembly and Properties of a Discrete Water-Soluble Prussian Blue Analogue Fe^{II}/Co^{III} Cube: Confinement of a Water Molecule in Aqueous Solution. *Inorganic Chemistry* **2020,** *59*, 1582-1587.
46. Bernhardt, P. V.; Bozoglián, F.; Macpherson, B. P.; Martínez, M.; Merbach, A. E.; González, G.; Sienra, B., Oxidation of Mixed-Valence Co^{III}/Fe^{II} Complexes Reversed at High pH: A Kinetico-Mechanistic Study of Water Oxidation. *Inorganic Chemistry* **2004,** *43*, 7187-7195.
47. Bernhardt, P. V.; Bozoglián, F.; Macpherson, B. P.; Martínez, M.; González, G.; Sienra, B., Discrete cyanide bridged mixed-valence Co/Fe complexes: outer sphere redox behaviour. *European Journal of Inorganic Chemistry* **2003**, 2512-2518.

48. Alcázar, L.; Bogdándi, V.; Lente, G.; Martínez, M.; Vázquez, M., Temperature- and Pressure-Dependent Kinetico-Mechanistic Studies on the Formation of Mixed-Valence {(Tetraamine)$Co^{III}NCFe^{II}(CN)_5$}$^-$ units. *Journal of Coordination Chemistry* **2015,** *60*, 3058-3068.
49. Bernhardt, P. V.; Martínez, M.; Rodríguez, C., Outer-Sphere Redox Reactions leading to the Formation of Discrete Co^{III}/Fe^{II} pyrazine-Bridged Mixed Valence Compounds. *European Journal of Inorganic Chemistry* **2010**, 5621-5629.
50. Bernhardt, P. V.; Martínez, M.; Rodríguez, C.; Vazquez, M., Discrete Rh^{III}/Fe^{II} and $Rh^{III}/Fe^{II}/Co^{III}$ Cyanide-Bridged Mixed Valence Compounds. *Inorganic Chemistry* **2011,** *50*, 1429-1440.
51. Basallote, M. G.; Bernhardt, P. V.; Calvet, T.; Castillo, C. E.; Font-Bardia, M.; Martínez, M.; Rodríguez, C., Mechanistic aspects of the chemistry of mononuclear Cr^{III} complexes with pendant-arm macrocyclic ligands and formation of discrete Cr^{III}/Fe^{II} and $Cr^{III}/Fe^{II}/Co^{III}$ cyano-bridged mixed valence compounds. *Dalton Transactions* **2009**, 9567-9577.
52. Bernhardt, P. V.; Bozoglián, F.; Font-Bardia, M.; Martínez, M.; Meacham, A. P.; Sienra, B.; Solans, X., The Influence of Ligand Substitution at the Electron Donor Center in Molecular Cyano-Bridged Mixed-Valent Co^{III}/Fe^{II} and Co^{III}/Ru^{II} Complexes. *European Journal of Inorganic Chemistry* **2007**, 5270-5276.
53. Bernhardt, P. V.; Boschloo, G. K.; Bozoglián, F.; Hagfeldt, A.; Martínez, M.; Sienra, B., Tailoring mixed-valence Co^{III}/Fe^{II} complexes for their potential use as sensitizers in dye sensitized solar cells. *New Journal of Chemistry* **2008,** *32*, 705-711.
54. Basallote, M. G.; Bozoglián, F.; Fernandez-Trujillo, M. J.; Martínez, M., Sol-gel materials with trapped trinuclear *class-ii* mixed-valence macrocyclic complexes that mimic their solution redox behaviour. *New Journal of Chemistry* **2008,** *32*, 264-272.
55. Bernhardt, P. V.; Macpherson, B. P.; Martínez, M., Discrete Dinuclear Cyano-Bridged Complexes. *Inorganic Chemistry* **2000,** *39*, 5203-5208.
56. No differences were observed when the spectrum was run on 0.1 M solutions of either NaCl or LiCl.
57. The sample was subsequently dissolved (after being taken to dryness) in non-deuterated water and no signal of encapsulated lithium/water units was oberved after one week, indicating that the exchange observed is not due to simple H/D or water scramble.
58. Pyykkö, P.; Riedel, S.; Patzschke, M., Triple-Bond Covalent Radii. *Chemistry – A European Journal* **2005,** *11*, 3511-3520.
59. Hong, T.; Zhang, Z.; Sun, Y., *et al.*, Chiral Metallacycles as Catalysts for Asymmetric Conjugate Addition of Styrylboronic Acids to α,β-Enones. *Journal of the American Chemical Society* **2020,** *142*, 10244-10249.
60. Tobe, M. L.; Burgess, J., *Inorganic Reaction Mechanisms*. Longman: New York, 1999.
61. Espenson, J. H., *Chemical Kinetics and Reaction Mechanisms*. McGraw-Hill: New York, 1981.
62. Wilkins, R. G., *Kinetics and Mechanisms of Reactions of Transition Metal Complexes*. VCH: Weinheim/New York, 1991.
63. Lappin, A. G., *Redox Mechanisms in Inorganic Chemistry*. Ellis Horwood: Chichester, 1994.
64. Martínez, M.; Pitarque, M. A.; van Eldik, R., Outer-sphere redox reactions of $[Co^{III}(NH_3)_5(H_xP_yO_z)]^{(m-3)-}$ complexes. A temperature- and pressure-dependence kinetic study on the influence of the phosphorus oxoanions. *Journal of the Chemical Society, Dalton Transactions* **1996**, 2665-2671.

65. Huchital, D. H.; Wilkins, R. G., A study of the intermediates formed in the reaction of ethylenediaminetetraacetatocobaltate(II) with ferricyanide ion. *Inorganic Chemistry* **1967,** *6*, 1022-1027.
66. Searle, G. H.; Wang, D. N.; Larsen, S.; Larsen, E., The Structure of a Novel Complex of Cobalt(III) with a Tridentate Macrocyclic Ligand with Tertiary Amine Donors, $[CoL(NCCH_3)_2Cl]CoCl_4$ (L = 1,4,7-Trimethyl-1,4,7-triazacyclononane). *Acta Chemica Scandinavica* **1992,** *46*, 38-42.
67. Alcázar, L.; Aullón, G.; Ferrer, M.; Martínez, M., Redox-Assisted Self-Assembly of a Water-Soluble Cyanido-Bridged Mixed Valence $\{Co^{III}/Fe^{II}\}_2$ Square. *Chemistry – A European Journal* **2016,** *22*, 15227-15230.
68. Herren, F.; Fischer, P.; Ludi, A.; Haelg, W., Neutron diffraction study of Prussian Blue, $Fe_4[Fe(CN)_6]_3.xH_2O$. Location of water molecules and long-range magnetic order. *Inorganic Chemistry* **1980,** *19*, 956-959.
69. Zhang, N.; Kawamoto, T.; Jiang, Y., *et al.*, Interpretation of the Role of Composition on the Inclusion Efficiency of Monovalent Cations into Cobalt Hexacyanoferrate. *Chemistry – A European Journal* **2019,** *25*, 5950-5958.
70. Tobe, M. L., *Inorganic Reaction Mechanisms*. Nelson: Sunbury on Thames, 1977.
71. Burgess, J., *Ions in Solution*. Albion/Horwood: Chichester, 1999.
72. Atkins, P.; Overton, T.; Rourke, J.; Weller, M.; Armstrong, F. A., *Inorganic Chemistry*. 4th ed.; Oxford University Press: 2006.
73. Greenwood, N.; Earnshow, A., *Chemistry of the Elements*. Second ed.; Butterworth-Heinemann: 1997.
74. Bernhardt, P. V.; Gonzálvez, M. A.; Martínez, M., Kinetico-mechanistic Study on the Oxidation of Biologically Active Iron(II) Bis(thiosemicarbazone) Complexes by Air. Importance of $NH\text{-}O_2$ Interactions As Established by Activation Volumes. *Inorganic Chemistry* **2017,** *56*, 14284-14290.
75. Martínez, M.; Vázquez, M., Kinetico-mechanistic studies of nucleoside and nucleotide substitution reactions of Co^{III} complexes of fully alkylated Cyclen. *Inorganic Chemistry* **2015,** *54*, 4972-4980.
76. Rafols, L.; Josa, D.; Aguilà, D., *et al.*, Piano-Stool Ruthenium(II) Complexes with Delayed Cytotoxic Activity: Origin of the Lag Time. *Inorganic Chemistry* **2021,** *60*, 7974-7990.
77. Mevissen, C.; Sommer, D.; Vasanthakumar, S.; Truong, K.-N.; Rissanen, K.; Albrecht, M., Cation-translocation based isomerism offers a tool for the expansion of compressed helicates. *Dalton Transactions* **2021,** *50*, 9372-9375.
78. van Eldik, R., High Pressure Kinetics; Fundamental and Experimental Aspects. In *Inorganic High Pressure Chemistry*, van Eldik, R., Ed. Elsevier: 1986; pp 1-68.
79. Crespo, M.; Font-Bardia, M.; Hamidizadeh, P.; Martínez, M.; Nabavizadeh, S. M., Kinetico-mechanistic study on the reduction/complexation sequence of Pt^{IV}/Pt^{II} organometallic complexes by thiol-containing biological molecules. *Inorganica Chimica Acta* **2019,** *486*, 8-16.
80. Mironov, V. E.; Pashkov, G. L.; Isaev, I. D.; Leont'ev, V. M.; Stupko, T. V., Effect of Ionic Strength, Nonaqueous Additives, and Temperature on Stability Constants of Sulfate Complexes of Pentaammineaquacobalt in Aqueous Solutions. *Russian Journal of Inorganic Chemistry* **1996,** *41*, 3.
81. M. J. Frisch; Trucks, G. W.; Schlegel, H. B., *et al. Gaussian09*, Gaussian Inc.: Wallingford CT, 2009.
82. Perdew, J. P.; Burke, K.; Ernzerhof, M., Generalized Gradient Approximation Made Simple. *Physical Review Letters* **1997,** *78*, 1396-1396.

83. Perdew, J. P.; Burke, K.; Ernzerhof, M., Generalized Gradient Approximation Made Simple. *Physical Review Letters* **1996,** *77*, 3865-3868.
84. Weigend, F.; Ahlrichs, R., Balanced basis sets of split valence, triple zeta valence and quadruple zeta valence quality for H to Rn: Design and assessment of accuracy. *Physical Chemistry Chemical Physics* **2005,** *7*, 3297-3305.
85. Weigend, F., Accurate Coulomb-fitting basis sets for H to Rn. *Physical Chemistry Chemical Physics* **2006,** *8*, 1057-1065.
86. Tannor, D. J.; Marten, B.; Murphy, R.; Friesner, R. A.; Sitkoff, D.; Nicholls, A.; Honig, B.; Ringnalda, M.; Goddard, W. A., Accurate First Principles Calculation of Molecular Charge Distributions and Solvation Energies from Ab Initio Quantum Mechanics and Continuum Dielectric Theory. *Journal of the American Chemical Society* **1994,** *116*, 11875-11882.
87. Marten, B.; Kim, K.; Cortis, C.; Friesner, R. A.; Murphy, R. B.; Ringnalda, M. N.; Sitkoff, D.; Honig, B., New Model for Calculation of Solvation Free Energies: Correction of Self-Consistent Reaction Field Continuum Dielectric Theory for Short-Range Hydrogen-Bonding Effects. *The Journal of Physical Chemistry* **1996,** *100*, 11775-11788.
88. Marenich, A. V.; Cramer, C. J.; Truhlar, D. G., Universal Solvation Model Based on Solute Electron Density and on a Continuum Model of the Solvent Defined by the Bulk Dielectric Constant and Atomic Surface Tensions. *The Journal of Physical Chemistry B* **2009,** *113*, 6378-6396.
89. Grimme, S.; Antony, J.; Ehrlich, S.; Krieg, H., A consistent and accurate ab initio parametrization of density functional dispersion correction (DFT-D) for the 94 elements H-Pu. *The Journal of Chemical Physics* **2010,** *132*, 154104.

For Table of Contents Only

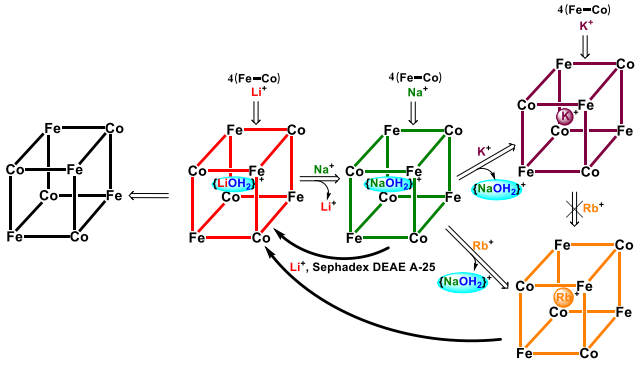

A series of alkali metal inclusion complexes of the molecular cube $[\{Co^{III}(Me_3\text{-tacn})\}_4\{Fe^{II}(CN)_6\}_4]\}]^{4-}$ has been achieved by following a redox-triggered self-assembly process. The alkali metals are encapsulated in an inert fashion as cationic $\{M–OH_2\}^+$ or M^+ units, which can be exchanged in a process that has been studied kinetico-mechanistically.